Sterol 14α-demethylase is vital for mitochondrial functions and stress tolerance in *Leishmania major*

Sumit Mukherjee[a*], Samrat Moitra[a], Wei Xu[a*], Veronica Hernandez[a] and Kai Zhang[a]#

[a]Department of Biological Sciences, Texas Tech University, Lubbock, TX 79409, USA.

*Current address: Department of Molecular Microbiology, Washington University School of Medicine, St. Louis, MO 63110, USA.

#Corresponding author: Kai Zhang, Department of Biological Sciences, Texas Tech University, Lubbock, TX 79409, USA. Tel: 1-806-834-0550. E-mail: kai.zhang@ttu.edu.

Short title: Sterol synthesis affects mitochondrial functions in *Leishmania*

ABSTRACT

Sterol C14-α-demethylase (C14DM) is a key enzyme in the biosynthesis of sterols and the primary target of azole compounds which show activities against trypanosomatids. In *Leishmania major*, genetic or chemical inactivation of C14DM leads to accumulation of 14-methylated sterol intermediates and profound plasma membrane abnormalities including increased fluidity and failure to maintain ordered membrane microdomains. These defects likely contribute to the hypersensitivity to heat and severely reduced virulence displayed by the C14DM-null mutants (*c14dm*$^{-}$). In addition to plasma membrane, sterols are present among intracellular organelles. In this study, we investigated the impact of C14DM ablation on mitochondria. Our results demonstrate that *c14dm*$^{-}$ mutants possess significantly higher mitochondrial membrane potential than wild type parasites. Such high potential leads to the buildup of reactive oxygen species in the mitochondria, especially under nutrient-limiting conditions. Consistent with these mitochondrial alterations, c*14dm*$^{-}$ mutants show impairment in respiration and are heavily dependent on glucose uptake and glycolysis to generate energy. Consequently, these mutants are extremely sensitive to glucose deprivation and such vulnerability can be rescued through the supplementation of glucose or glycerol. Finally, besides plasma membrane defects, the accumulation of oxidants may also contribute to the hypersensitivity to heat exhibited by *c14dm*$^{-}$. In summary, our investigation reveals that alteration of sterol synthesis can negatively affect multiple cellular processes in *Leishmania* parasites and sensitize them to clinically relevant stress conditions.

AUTHOR SUMMARY

Sterols are well recognized for their stabilizing effects on the plasma membrane, but their functions in intracellular organelles are poorly understood, which hampers the development of sterol synthesis inhibitors as drugs. Our previous studies have demonstrated significant plasma membrane instability in the sterol biosynthetic mutant *c14dm*$^{-}$ in *Leishmania major*, a pathogenic protozoan responsible for cutaneous leishmaniasis causing 1-1.5 million infections a year. While the plasma membrane defects have undoubtedly contributed to the reduced virulence exhibited by *c14dm*$^{-}$ mutants, it was not clear whether other cellular processes were also affected. In this study, we revealed profound mitochondrial dysfunctions and elevated level of reactive oxygen species in *c14dm*$^{-}$ mutants. Rather than respiration, these sterol mutants primarily rely on glycolysis to generate energy and are extremely sensitive to glucose restriction. In addition, the accumulation of oxidants appears to be responsible (at least in part) for the previously observed heat sensitivity in *c14dm*$^{-}$ mutants. Thus, genetic or chemical inactivation of C14DM can influence the functions of cellular organelles beyond the plasma membrane. These findings shed light on the mechanism of action of azole compounds and provide new insight into the roles of sterol biosynthesis in *Leishmania* parasites.

INTRODUCTION

Parasitic protozoa of the genus *Leishmania* are the causative agents for a group of diseases in humans and animals known as leishmaniasis [1, 2]. During their life cycle, *Leishmania* parasites alternate between flagellated, extracellular promastigotes in sandfly vectors and non-flagellated, intracellular amastigotes in vertebrates. Current drugs for leishmaniasis are plagued with high toxicity, low efficacy and resistance is on the rise [3]. Therefore, research involving the identification and characterization of metabolic pathways that could provide new drug targets is of significant value.

While mammalian cells synthesize cholesterol as the main sterol, *Leishmania* promastigotes primarily make ergostane-based sterols such as ergosterol and 5-dehydroepisterol [4-6]. Ergosterol is distinguished from cholesterol by the presence of an unsaturated side chain with a methyl group at the C24 position and an additional double bond at C7-C8 in the B ring of the sterol core. Differing from promastigotes, *Leishmania* amastigotes (which reside in macrophages) mainly salvage cholesterol from the host, while downregulating the de novo ergosterol synthesis [7]. Despite the low abundance of ergostane-based sterols in amastigotes, sterol synthesis inhibitors have shown promise as anti-leishmaniasis drugs [5, 8, 9], suggesting that the residue amount of endogenous sterols are crucial for amastigotes or the accumulation of sterol intermediates is detrimental. Among these sterol synthesis inhibitors are azole compounds which primarily target the cytochrome P450 enzyme sterol C14-α-demethylase (C14DM) [5, 10, 11]. Contribution of sterol biosynthesis to *Leishmania* biology is not fully understood, which hinders the development and improvement of azoles as anti-leishmaniasis drugs.

C14DM was found to be refractory to genetic deletion in *Leishmania donovani*, the causative agent for visceral leishmaniasis [12]. In contrast, our earlier study showed that this

enzyme was dispensable in *Leishmania major* (responsible for cutaneous leishmaniasis in the old world) [7]. Thus, different *Leishmania* species may possess distinct requirements for sterol synthesis. Importantly, although *L. major* C14DM-null mutants (*c14dm*¯) are viable as promastigotes under normal tissue culture conditions, they display increased plasma membrane fluidity, disorganization in lipid raft formation, and deficiency in lipophosphoglycan (LPG, a major surface glycoconjugate and virulence factor [13]) synthesis [7]. These plasma membrane defects probably contribute to the mutants' hypersensitivity to heat and their severely attenuated virulence in mice, although other factors may be involved as well [7]. Further studies indicate that the accumulation of aberrant, 14-methylated sterol intermediates, not the lack of ergostane-based sterols, is mainly responsible for the fitness loss displayed by *c14dm*¯ mutants [14].

While sterols are well recognized for their stabilizing effects on the plasma membrane [15, 16], their functions in intracellular organelles are poorly understood, as the end products of sterol synthesis are mainly found on the plasma membrane and secretory vesicles in mammalian cells and yeast [17-19]. In *L. major*, C14DM is primarily found in the ER but also present in the mitochondria suggesting this enzyme is needed there [7]. An earlier study reported the presence of substantial amounts of endogenous and exogenous sterols in the mitochondria of *Trypanosoma cruzi*, a related trypanosomatid protozoan [20]. Application of sterol biosynthesis inhibitors such as ketoconazole and lovastatin affected the ultrastructure of mitochondria in *T. cruzi*, leading to intense proliferation of the inner-mitochondrial membranes and necrotic cell death [21]. Similarly, RNAi knockdown of ergosterol pathway genes in *Trypanosoma brucei* resulted in disorganization of mitochondria structure and depletion of ATP production [22]. In *Leishmania*, the lipid composition of mitochondrial membrane has yet to be determined. Nonetheless, structural and functional abnormalities were also observed among other defects

following treatment with azole compounds. For example, in *Leishmania amazonensis*, combinatorial treatment of ketoconazole and terbinafine led to alterations in the distribution and appearance of cristae and the formation of paracrystalline arrays within the mitochondrial matrix [23]. Another study reported the collapse of mitochondrial membrane potential (ΔΨm) following posaconazole treatment in *L. amazonensis* [24]. Besides azoles, treatment of *L. amazonensis* and *T. cruzi* with various azasterols, which inhibit the sterol C24-methyltransferase, induced a loss of mitochondrial matrix contents [21, 25, 26]. Although the off-target effects from inhibitors cannot be excluded, these observations suggest that sterol synthesis play important roles in preserving the structure and function of mitochondria in trypanosomatids.

Compared to mammalian cells which usually possess multiple mitochondria per cell, trypanosomatids parasites have only one, relatively large mitochondrion per cell [27]. In addition to energy production, mitochondria in trypanosomatids have been implicated in fatty acid synthesis and redox homeostasis during different stages of their life cycle [28, 29]. Mitochondrial malfunctions, e.g. changes in ΔΨm, disruption of mitochondrial membrane integrity, and increase in reactive oxygen species (ROS) production, are major mediators of cell death under various stress conditions [30-32].

In this study, we sought to address the following important questions. First, how does C14DM inactivation affect the integrity and functions of mitochondria in *L. major*? Second, besides heat sensitivity, do *c14dm*$^-$mutants exhibit any other stress response defects? Third, how do mitochondrial deficiencies influence the fitness of *c14dm*$^-$parasites? Our results showed that genetic or chemical disruption of C14DM severely compromised the mitochondria in *L. major*, leading to significant ROS accumulation and extreme vulnerability to biologically relevant stress

conditions such as heat and glucose starvation. These findings may guide the development of new treatment strategies that exploit the fitness cost associated with drug resistance.

RESULTS

C14dm⁻ promastigotes show increased mitochondrial membrane potential (ΔΨm) and altered mitochondrial morphology.

To examine if C14DM deletion affects the mitochondria in *L. major*, we labeled promastigotes with MitoTracker CMXRos, a fluorogenic dye that binds to mitochondria in a ΔΨm-dependent manner. As indicated in Fig 1A, *c14dm⁻* mutants showed an intense mitochondrial staining 2-4 times stronger than WT and *c14dm⁻*/+C14DM (add-back) parasites. In addition, the mitochondria of *c14dm⁻* appeared to be more swollen with larger volume and surface area based on transmission electron microscopy and quantitative analysis by fluorescence microscopy (Fig 1B and Fig S1A). To examine whether the mitochondrial membrane in *c14dm⁻* was compromised, we analyzed the presence of cytochrome *c* in mitochondrial fraction and cytosolic fraction following extraction with digitonin, with ISCL and HSP83 being used as mitochondrial and cytosolic markers, respectively [33] [34](Fig S1B). Similar to WT and *c14dm⁻*/+C14DM parasites, cytochrome *c* in *c14dm⁻* remained in the mitochondrial enriched fractions when the digitonin extraction was performed at room temperature (Fig S1B). As a control, digitonin treatment at 37 °C disrupted the outer mitochondrial membrane, causing cytochrome *c* release into the cytosol [35] (Fig S1B). Thus, despite of its effects on ΔΨm and mitochondrial size, genetic ablation of C14DM does not affect mitochondrial membrane integrity at least with regard to cytochrome *c* localization under ambient conditions.

Consistent with the MitoTracker staining results, when live parasites were labeled with another ΔΨm-dependent dye tetramethylrhodamine ethyl ester (TMRE), *c14dm⁻* mutants retained 2-4 times more fluorescence than WT and *c14dm⁻/+C14DM* cells as indicated by flow cytometry and microscopy (Fig 1C-1D). The difference between WT and *c14dm⁻* parasites was

more pronounced during the log phase when cells were metabolically active than stationary phase (Fig 1C). Similar results were observed after staining with rhodamine 123 (Fig S2). As expected, pretreatment with the mitochondrial uncoupler CCCp (75 μM for 15 min) dramatically reduced the incorporation of TMRE and MitoTracker into WT and *c14dm*$^{-}$parasites (Fig 1A and 1C), without significant effect on cell viability (<5% of cells were propidium iodide positive by flow cytometry). Furthermore, WT promastigotes grown in the presence of itraconazole (ITZ, a C14DM inhibitor) [7] for 48 hours at sublethal concentrations showed similar ΔΨm as *c14dm*$^{-}$ mutants (Fig 1C). Finally, we also examined if extracellular nutrient level affects ΔΨm by labelling promastigotes with TMRE in either complete M199 medium, M199 medium without fetal bovine serum, phosphate-buffered saline (PBS) supplemented with 5.5 mM of glucose (the glucose concentration in M199 medium), or PBS alone (Fig 2A). In these experiments, *c14dm*$^{-}$ mutants exhibited 2.5-4 times higher ΔΨm than WT/add-back parasites and no significant differences were detected between nutrient-replete and nutrient limiting conditions (Fig 2A). Collectively, these observations suggest that C14DM inhibition leads to significantly increased ΔΨm in *L. major* promastigotes regardless of extracellular nutrient levels.

Inactivation of C14DM leads to ΔΨm-dependent accumulation of ROS in the mitochondria.

In mammalian cells, a high ΔΨm may cause accumulation of ROS in the mitochondria (mainly in the form of superoxide or $O_2^{\bullet-}$) in part due to reverse electron flow from complex II to complex I of the electron transport chain (ETC) [36-38]. To assess the ROS level in *c14dm*$^{-}$ mutants, promastigotes were labelled with a mitochondria-specific ROS indicator MitoSox Red which binds to mitochondrial nucleic acid and fluoresces upon oxidation by superoxide [39]. In complete M199, *c14dm*$^{-}$mutants showed 3.5 times more MitoSox labeling than WT and add-back cells (Fig 2B). Unlike ΔΨm, the mitochondrial ROS level in *c14dm*$^{-}$parasites was sensitive

to nutrient availability: PBS only > PBS with glucose > M199 medium without fetal bovine serum > complete M199 (Fig 2B). Importantly, pretreatment of *c14dm*⁻parasites with CCCp significantly reduced MitoSox Red labeling, indicating that the high ΔΨm is mainly responsible for ROS accumulation (Fig 2A-B and Fig 1C). These findings suggest that the mitochondria in *c14dm*⁻mutants are under significant oxidative stress during starvation.

Next we examined the mitochondrial ROS levels in log phase and stationary phase promastigotes after labeling them with MitoSox in PBS alone (Fig 2C). Compared to WT and add-back cells, *c14dm*⁻mutants contained 10-15 times more mitochondrial ROS by flow cytometry during log phase and early stationary phase, and the difference became less dramatic during late stationary phase when cells ceased proliferation (Fig 2C). Microscopic examination of MitoSox-labelled parasites revealed singular fluorescent spots in every cell representing the kinetoplast DNA, indicating the mitochondrial origin of ROS (Fig 2D). In addition, MitoSox signals from *c14dm*⁻were much more prominent than those from WT and *c14dm*⁻*/+C14DM* cells (Fig 2D), which was in agreement with flow cytometry analysis (Fig 2B-C). Furthermore, when cultivated in the presence of ITZ (at 0.1-0.2 µM or near EC25 levels), *L. major* WT promastigotes and *L. mexicana* axenic amastigotes displayed high levels of MitoSox Red staining similar to *c14dm*⁻(Fig 2C and 2E), indicating that C14DM inhibition causes ROS built-up in the mitochondria of *Leishmania* parasites.

We also determined the cytoplasmic ROS level in *c14dm*⁻by labeling log phase parasites with dihydroethidium (DHE), a cytosolic ROS indicator. As illustrated in Fig 2F, the amount of cytosolic ROS in *c14dm*⁻was about two-fold higher than WT and add-back parasites, which was less dramatic than mitochondrial ROS. As a control, treatment of WT parasites with hydrogen peroxide (100 µM for 10 min) led to significantly increased staining for DHE but not MitoSox

Red, confirming the specificity of MitoSox Red for mitochondrial superoxide (Fig S3). Together, these data suggest that genetic or chemical ablation of C14DM leads to significant accumulation of ROS inside the mitochondria.

Examination of superoxide dismutase (SOD) expression in *c14dm⁻* mutants.

Increases in ΔΨm and mitochondrial ROS were also observed in the sterol methyltransferase-null mutant *smt⁻*[14], although not as profound as the *c14dm⁻* mutant, suggesting that the accumulation of 14-methlyated sterol intermediates is mainly responsible for the mitochondrial alterations. As byproducts of mitochondrial respiration, ROS (mainly the form of $O_2^{\bullet-}$) can be generated from the partial reduction of oxygen by complexes I, II, and III of the ETC [40]. To limit the damaging effects of ROS, *Leishmania* cells utilize several antioxidant systems involving superoxide dismutases (SODs) and tryparedoxin peroxidases [41, 42]. The fact that *c14dm⁻* parasites accumulate high levels of $O_2^{\bullet-}$ suggests that either the ROS removal system is defective, or the production of $O_2^{\bullet-}$ is elevated due to excessive electron leakage from the ETC in these mutants. Here we examined whether the dysregulation of SOD, the primary enzyme to detoxify $O_2^{\bullet-}$, is responsible for the accumulation of mitochondrial ROS in *c14dm⁻*. *Leishmania* encode three iron-dependent SODs: the mitochondrial SODA and two glycosomal SODB (SODB1 and SODB2) [42, 43]. In whole cell lysate, we detected a 14-98% increase in SOD activity from *c14dm⁻* mutants and the increase was more pronounced during the stationary phase (Fig 3A). Western blot revealed that *c14dm⁻* mutants had similar levels of SODA (mitochondrial) and SODB (cytosolic) protein as WT parasites (Fig 3B). The increase in SOD activity in late stationary phase *c14dm⁻* coincided with the decrease of mitochondrial ROS (although still higher than WT and add-back parasites, Fig 2C and 3A), suggesting a compensatory response utilized by the mutants to upregulate their antioxidant defense machinery.

Collectively, these findings indicate that the ROS is accumulated in *c14dm*⁻ mutants despite of near- normal SOD production.

_C14dm_⁻ mutants display altered cellular respiration and increased glycolytic ATP production.

The mitochondrial abnormalities from *c14dm*⁻ prompted us to examine if these mutants could effectively carry on respiration and generate ATP. First we measured the cellular oxygen consumption rate using the MitoXpress oxygen probe as described previously [44]. When incubated a mitochondrial respiration buffer made of Hanks' balanced salt solution (HBSS) containing sodium pyruvate and 2-deoxyglucose (to block glycolysis) [45], *c14dm*⁻ parasites showed a significant reduction (42-60%) in oxygen consumption compared to WT cells, and such defect was corrected in the *c14dm*⁻/+C14DM parasites (Fig 4A). The low oxygen consumption rate may protect *c14dm*⁻ parasites from further ROS accumulation. As expected, treatment of WT parasites with antimycin A, a respiratory inhibitor that blocks cytochrome *c* reductase or complex III [46], decreased the cellular oxygen consumption (Fig 4A).

Next, we determined the ATP production from WT, *c14dm*⁻ and *c14dm*⁻/+C14DM parasites. When log phase promastigotes were incubated in HBSS buffer without glucose for 1 hour, no significant difference in ATP content was observed in *c14dm*⁻ relative to WT and add-back parasites (Fig 4B). Supplementation with glucose led to increased ATP production in all cells, presumably from both glycolysis and mitochondrial respiration (Fig 4B). Importantly, despite the low oxygen consumption, *c14dm*⁻ mutants produced more ATP than WT and add-back parasites from glucose (Fig 4B), suggesting that these cells have increased capacity to carry out glycolysis. Addition of sodium azide which inhibits cytochrome *c* oxidase [45, 47] significantly reduced ATP production in WT parasites, yet the effect was less severe in *c14dm*⁻

mutants (Fig 4B), which is consistent with the notion that these mutants are less dependent on respiration to generate energy.

We also measured the ATP contents in cells incubated in HBSS buffer containing sodium pyruvate but no glucose (Fig 4C). While no significant difference between WT and *c14dm*$^-$ parasites was detected after 1 hour, longer incubation (4 hours) led to significantly less intracellular ATP in *c14dm*$^-$ (Fig 4C). This result suggests that in the absence of extracellular glucose, *c14dm*$^-$ mutants have difficulty producing energy (because of mitochondrial defects) after intracellular nutrients are depleted.

Glucose starvation has deleterious effect on *c14dm*$^-$ parasites.

Our findings so far suggest that *c14dm*$^-$ parasites primarily depend on non-respiration pathways such as glycolysis to generate energy. If so, these mutants would be highly sensitive to glucose restriction. To test this possibility, we exposed parasites to glucose-limiting conditions and measured cell survival over time. As illustrated in Fig 5A-B, when incubated in HBSS, *c14dm*$^-$ mutants showed substantial cell death after 8-12 hours. At 20-24 hours, more than 90% of *c14dm*$^-$ cells were dead (Fig 5A-B). Similar results were observed when parasites were incubated in other neutral, isotonic buffers such as PBS (Fig S4 and data not shown). In addition, *L. major* WT parasites cultivated in the presence of ITZ were highly vulnerable to glucose starvation like *c14dm*$^-$ mutants (Fig S5). In these experiments, WT control, *smt*$^-$, *smt*$^-$/+SMT and *c14dm*$^-$/+C14DM parasites showed very good survival (<9% death after 24 hours), indicating this phenotype is caused by the ablation of C14DM (Fig 5A and data not shown). Importantly, supplementation with glucose at 5.5 mM (the glucose concentration in M199 medium) completely rescued *c14dm*$^-$ mutants, whereas at the same molar concentration, sodium pyruvate (a respiration substrate), 2-deoxyglucose (a non-metabolizable glucose analog), or aspartate (a

gluconeogenic amino acid) failed to protect the mutants (Fig 5A). Further tests revealed that glucose concentrations above 100 µM were sufficient to rescue *c14dm⁻* mutants (Fig S4 and data not shown).

Recent studies have revealed that bloodstream forms of *Trypanosoma brucei* can use glycerol to support growth in the absence of glucose [48, 49]. To test if *Leishmania* parasites can utilize glycerol effectively, we attempted to rescue *c14dm⁻* mutants with glycerol. Remarkably, when provided at more than 100 µM, glycerol was able to protect *c14dm⁻* mutants under glucose-free conditions (Fig 5A-B and Fig S4). Both glucose and glycerol were also able to alleviate the mitochondrial defects in *c14dm⁻* mutants (Fig S6). Together, our results indicate that inactivation of C14DM leads to hypersensitivity to glucose starvation, which is likely caused by energy depletion and excessive ROS accumulation.

***C14dm⁻* parasites show increased uptake of glucose and glycerol.**

Next we examined whether the uptake of glucose and glycerol is altered in *c14dm⁻* parasites using radiolabeled substrates as previously described [50, 51]. If respiration defects force *c14dm⁻* mutants to rely more on glycolysis to generate energy, these parasites may have higher demands for glucose or equivalent carbon sources. Trypanosomatid protozoans including *Leishmania* species possess a family of glucose transporters [52] and aquaglyceroporins [51] that can mediate nutrient uptake. As shown in Fig 6, *c14dm⁻* mutants were more efficient than WT and add-back parasites in the uptake of glucose and glycerol. The incorporation of glucose was much more robust at room temperature than at 4 °C (Fig 6A), whereas the incorporation of glycerol was less dependent on temperature (Fig 6B-C). The increased uptake of glucose and glycerol in *c14dm⁻* may serve as a compensatory mechanism to offset deficiencies in mitochondrial respiration.

ROS accumulation is partially responsible for the heat sensitivity in *c14dm⁻* mutants.

We have previously shown that *c14dm⁻* parasites are extremely sensitive to heat stress (e.g. 37 °C treatment), and their increased plasma membrane fluidity (induced by the accumulation of 14-methylated sterol intermediates) is a likely cause [7]. To investigate if the accumulation of ROS is also a contributing factor, WT and *c14dm⁻* parasites were incubated in PBS at either 27 °C (the regular temperature for promastigotes) or 37 °C. After 3 hours, a marked reduction in ΔΨm was detected in 30-35% of *c14dm⁻* parasites without substantial cell death (Fig 7A-B). No significant change in ΔΨm was observed in WT parasites (Fig 7B). To determine if the loss of ΔΨm was associated with compromised mitochondrial membrane integrity, we assessed the release of cytochrome *c* from mitochondria into the cytosol (Fig 7C-D). For WT cells, the majority of cytochrome *c* was found in the mitochondrial enriched membrane fractions under control (27 °C) and heat treatment (37 °C, 3 hours) conditions (Fig 7C-D). In contrast, ~40% of cytochrome *c* was detected in the cytosolic fraction when *c14dm⁻* parasites were subjected to heat treatment (Fig 7C-D). Again, 3 hours at 37 °C did not induce substantial cell death (Fig 7A), indicating the mitochondrial disruption occurs when the majority of *c14dm⁻* mutants are viable. In addition, we measured the levels of cytosolic ROS in control and heat stressed cells. Unlike WT and add-back parasites which showed no significant change, *c14dm⁻* mutants displayed ~3-fold increase in cytosolic ROS following 37 °C treatment for 3 hours (Fig 7E). Together, these data suggest that heat stress causes a partial rupture of mitochondrial outer membrane in *c14dm⁻*, leading to the dissemination of cytochrome *c* and ROS into the cytosol.

To further evaluate the contribution of ROS accumulation to the observed heat response phenotype, we treated *c14dm⁻* mutants with glutathione (GSH, an antioxidant) before exposing them to 37 °C. When administered at 5 mM, GSH treatment of *c14dm⁻* reduced the

mitochondrial ROS by ~60% and the heat-induced cell death in 8 hours by ~50% (Fig 7F-G). The effect was much less prominent when GSH was provided at 1 mM (Fig 7F-G), indicating a dosage-dependent reverse of ROS stress. Finally, we tested the effect of antimycin A, an oxidative stress inducer (Fig S3A), on the heat sensitivity of WT parasites. At 27 °C, 10 µM of antimycin A had very mild effect on cell survival (<10% death after 36 hours) but at 37 °C, more than 60% of WT cells died after 8 hours (Fig 7H). From these studies, we conclude that in addition to plasma membrane defects, oxidative stress also makes *c14dm*$^{-}$mutants vulnerable to heat.

DISCUSSION

Our previous work has revealed significant plasma membrane defects in *c14dm*⁻mutants including increased membrane fluidity and failure to maintain detergent resistant membrane fractions. While predominantly located in the plasma membrane, sterols are also present in substantial amounts in lipid droplets and intracellular organelle membranes [19, 53]. A more thorough characterization of the *c14dm*⁻mutants would reveal new insight into the roles of sterol metabolism in *Leishmania* and provide new leads to exploit the vulnerability caused by abnormal sterols. In this study, we found a 2-5 folds increase in the ΔΨm of *c14dm*⁻relative to WT and add-back parasites and similar results were observed in ITZ-treated WT parasites (Fig 1 and Fig S2). We also detected a modest swelling of mitochondria in *c14dm*⁻mutants (Fig 1B and Fig S1A). These findings are consistent with the previously reported hyperpolarization of mitochondrial membrane in *Leishmania mexicana* following treatment with triazole compounds [54].

In mammalian cells, elevated ΔΨm may cause electron flow in the reverse direction through the ETC leading to electron leakage and superoxide accumulation in the mitochondrial matrix [36, 38]. By flow cytometry and fluorescence microscopy, we observed significantly higher levels of superoxide in the mitochondria of *c14dm*⁻mutants and ITZ-treated WT parasites in comparison to control cells (Fig 2 and Fig S3). Under the nutrient-replete condition, a 3-5-fold increase was detected in *c14dm*⁻mutants. Under the nutrient-limiting condition, the difference became 10-12-fold (Fig 2B). Meanwhile, the cytosolic ROS level in *c14dm*⁻mutants was only about 2-fold higher than WT and add-back parasites, suggesting that the majority of accumulated ROS was sequestered in the mitochondria under ambient temperature (Fig 2F and Fig S3). In agreement with this notion, the mitochondrial membrane integrity in *c14dm*⁻was confirmed by

examining the intracellular distribution of cytochrome *c* (Fig S1B). It is not clear why inactivation of C14DM leads to elevated levels of ΔΨm and mitochondrial ROS. The expression and activity of SODs were not compromised in *c14dm*⁻ mutants (Fig 3), suggesting that ROS production was higher in the absence of C14DM. In mammalian cells and yeast, mitochondria can synthesize phosphatidylglycerol (PG), cardiolipin (CL), phosphatidic acid, and a portion of phosphatidylethanolamine (PE, through the decarboxylation of phosphatidylserine) [18, 55, 56]. Other lipids including phosphatidylcholine, sphingolipids and sterols have to be imported. Changes in mitochondrial lipidome, especially the abundance of CL and PE, can lead to ETC defects [57, 58]. It is therefore possible that defects in sterol synthesis at the ER alter the lipid composition of mitochondrial membrane in *c14dm*⁻ mutants. Such membrane modification may negatively affect the functions of ETC including the terminal F0-F1 complex, leading to the accumulation of proton motive force (ΔΨm), leakage of electron and partial reduction of oxygen.

Additionally, when provided with sodium pyruvate, a mitochondrial respiratory substrate, *c14dm*⁻ parasites showed significant impairment of cellular oxygen consumption and reduced mitochondrial ATP production after 4 hours (Fig 4). Importantly, the overall ATP content in *c14dm*⁻ mutants was slightly higher than WT and add-back parasites when cells were incubated in the presence of glucose (Fig 4). These results suggest that without C14DM, *Leishmania* parasites downregulate respiration and primarily rely on glycolysis to generate energy. Mechanism of this energetics switch remains to be determined. In many eukaryotes, the heterotrimeric AMP-activated protein kinase (AMPK) complex is a key regulator of cellular energy metabolism [59-61]. Future investigation will examine if AMPK activation in response to C14DM ablation is responsible for increased glucose consumption via glycolysis.

Consistent with the increased dependency on glucose as an energy source, *c14dm⁻* mutants were extremely sensitive to glucose starvation (Fig 5). This hypersensitivity may arise from the lack of energy production as glucose is being depleted and the rapid increase in cellular ROS due to respiration deficiency (Fig 2 and Fig 5). An alternative and not mutually exclusive explanation is that the accumulation of aberrant sterol intermediates in *c14dm⁻* mutants compromised the progression of autophagy, a possibility currently under investigation. Interestingly, supplementation of either glucose or glycerol at concentrations above 100 μM completely rescued the survival of *c14dm⁻* mutants (Fig 5 and Fig S4). While glycerol could be converted into glucose, it is unlikely to account for the rescue as the energy required for gluconeogenesis exceeds that generated from glycolysis. Instead, it is possible that *Leishmania* parasites metabolize glycerol into glycerol-3-phosphate (by glycerol kinase) and then dihydroxyacetone phosphate (by the mitochondrial FAD-dependent glycerol-3-phosphate dehydrogenase) which can be incorporated into the glycolysis pathway, as described in *T. brucei* [48, 49]. We also observed increased uptake of glucose and glycerol by *c14dm⁻* mutants (Fig 6), a likely adaptive response to their high demand for carbon sources. Future research will focus on effects on sterol synthesis on the permeability of plasma membrane to probe the mechanism of this phenotype.

Finally, we examined the involvement of mitochondrial defects in the previously reported heat sensitivity exhibited by *c14dm⁻* mutants. Despite the high mitochondrial ROS, *c14dm⁻* parasites were fully viable at ambient temperature in the presence of glucose or glycerol. However, within 3 hours of exposure at 37 °C, the $\Delta\Psi m$ in *c14dm⁻* mutants showed signs of collapse, along with a significant increase in cytosolic ROS level and the release of cytochrome *c* to the cytosol (Fig 7). One possibility is that similar to the effect on plasma membrane, the

accumulation of aberrant sterol intermediates compromises the mitochondrial membrane integrity at high temperature in *c14dm⁻* parasites. Although the presence of a canonical apoptotic pathway in *Leishmania* is debatable, earlier studies have suggested the involvement of mitochondrial contents such as cytochrome *c* in causing cell death [31, 62]. In addition, treatment with antioxidant GSH could partially rescue the heat induced cell death *c14dm⁻* mutants, and the ROS generating agent antimycin A made WT *L. major* vulnerable to heat (Fig 7). Together, these findings suggest that ROS accumulation is partially responsible for the heat sensitivity in *c14dm⁻* parasites.

In summary, we have shown that deletion or inhibition of C14DM leads to significant alterations in the mitochondria highlighted by increases in ΔΨm and ROS levels, along with deficiency in respiration. These defects make *c14dm⁻* extremely vulnerable to glucose restriction and contribute to their hypersensitivity to heat. Thus, in addition to its stabilizing effects on the plasma membrane, sterol synthesis plays important roles in the regulation of cellular energetics, redox homeostasis and parasite fitness under stress. Analysis of the dynamics of ER-mitochondria transport, the mitochondrial lipid composition, and the spatial distributions and activities of ETC complexes in *c14dm⁻* would shed light on the mechanistic aspect of how endogenous sterols influence mitochondria in *Leishmania*. Finally, the *c14dm⁻* parasites were highly sensitive to pentamidine (Fig 8), whose uptake and activity seemed to be dependent upon the ΔΨm [63, 64]. This finding is in agreement with previous reports showing Amp B-resistant sterol mutants are hypersensitive to pentamidine [65, 66]. These results raise the possibility of using triazole/pentamidine or Amp B/pentamidine combinations against leishmaniasis. Future characterization of mitochondria in the clinically more relevant amastigote forms would provide

additional insights for the development of new treatment strategies, e.g. the application of glycolysis inhibitors and ROS inducers in conjugation with sterol biosynthesis inhibitors.

MATERIALS AND METHODS

Materials

Tetramethylrhodamine ethyl ester (TMRE), rhodamine 123, Mitotracker CMXRos, MitoSox Red, and dihydroethidium (DHE) were purchased from Thermo Fisher Scientific. Itraconazole (ITZ) was purchased from LKT Laboratories. Antimycin A was from ENZO Life Sciences. The MitoXpress oxygen consumption assay kit was purchased from Luxcel Biosciences. For ATP analysis, the CellTiter-Glo luminescent assay kit was purchased from Promega. All other chemicals were purchased from VWR International or Sigma Aldrich Inc. unless otherwise specified.

Leishmania culture

L. major LV39 clone 5 WT (Rho/SU/59/P), *c14dm*$^{-}$(C14DM-null mutant), and *c14dm*$^{-}$/+C14DM (episomal add-back) promastigotes were cultivated at 27 °C in complete M199 medium (M199 medium with 10% fetal bovine serum or FBS and additional supplements, pH 7.4) [67]. *Leishmania mexicana* (MNYC/BZ/62/M379) axenic amastigotes were cultured using an amastigote medium based on the Drosophila Schneider's medium supplemented with 20% FBS and 0.0015% hemin (pH 5.5) in vented flasks in a humidified 32 °C/5% CO_2 incubator [68]. Culture density and cell viability were determined by hemacytometer counting and flow cytometry after propidium iodide (PI)-staining, respectively as previously described [69]. In general, log phase promastigotes refer to replicative parasites at densities lower than 1.0 x 10^7 cells/ml, and stationary phase promastigotes refer to non-replicative parasites at densities higher than 2.0 x 10^7 cells/ml.

Determination of mitochondrial membrane potential (ΔΨm) and reactive oxygen species (ROS) level

ΔΨm was determined by flow cytometry after staining with TMRE or rhodamine 123 as previously described [70]. Briefly, promastigotes were resuspended in complete M199, serum-free M199, phosphate buffered saline (PBS, pH 7.2) containing 5.5 mM of glucose, or PBS alone at 2 x 10^6 cells/ml; TMRE was added to a final concentration of 100 nM; after incubation at 27 °C for 15 min, the mean fluorescence intensity (MFI) was determined using an Attune® NxT Flow Cytometer. Control samples include WT and *c14dm*⁻parasites pretreated with 75 µM of carbonyl cyanide m-chlorophenyl hydrazone (CCCp) for 15 min and WT parasites grown in the presence of 0.5 µM of ITZ for 48 hours.

Mitochondrial superoxide accumulation was determined as described previously with minor modifications [32]. Promastigotes were resuspended in complete M199, serum-free M199, PBS containing 5.5 mM of glucose, or PBS alone at 1 x 10^7 cells/ml and labeled with 5 µM of MitoSOX red at 27 °C. After 25 min, MFI was measured by flow cytometry as described above. To examine the level of cytosolic ROS, parasites were labeled with 5 µM of DHE for 30 min at 27 °C followed by flow cytometry analysis. Similar experiments were performed with cells labeled with 50 µM of CM-H_2DCFDA to measure total cellular ROS levels. Parasites pretreated with 5 µM of antimycin A, 75 µM of CCCp, or 100 µM of H_2O_2 for 15 min were used in these assays as controls. Such treatments did not affect parasite viability based on PI-staining (<5% PI positive). *C14dm*⁻mutants grown in the presence of 1 mM or 5 mM of glutathione (GSH) for 48 hours were also included. In all flow cytometry experiments, 20,000 events were acquired for each sample.

Determination of superoxide dismutase (SOD) activity

SOD activity in whole cell extracts was measured as described previously for *L. amazonensis* [71]. Briefly, 2 x 10^8 promastigotes were harvested, washed twice with PBS and

resuspended in a hypotonic buffer (5 mM of Tris–HCl, 0.1 mM of EDTA, and 1 x complete EDTA-free protease inhibitor cocktail, pH 7.8) at a final concentration of 5 x 10^8 cells/ml. To prepare lysates, cells were subjected to three freeze-thaw cycles alternating between liquid nitrogen and a 37 °C water bath. Cell lysis was confirmed by microscopy. Lysates were clarified by centrifugation (12000 g for 30 min at 4 °C) and protein concentrations were determined using a BCA protein assay kit (Thermo Fisher Scientific). SOD activity in whole cell extracts was measured using the EnzyChrome superoxide dismutase assay kit (BioAssay Systems) according to the manufacturer's protocol.

Digitonin fractionation and Western blot

Crude mitochondria-enriched fractions were generated by digitonin fractionation as described previously [72]. Briefly, log phase promastigotes were incubated for 10 min on ice in 20 mM of Tris-HCl pH 7.5, 0.6 M of sorbitol, 2 mM of EDTA and 0.025% (w/v) of digitonin at 1 x 10^8 cells/ ml at room temperature. As a positive control for mitochondrial membrane disruption, WT parasites were treated with 0.035% (w/v) of digitonin at 37 °C. After centrifugation (8000 g, for 30 min at 4 °C), the resulting mitochondria-enriched pellet was separated from the supernatant (enriched for cytosolic proteins). Fractions of equal cell equivalents were subjected to SDS-PAGE and immunoblotting. Primary antibodies included rabbit-anti-*T. brucei* cytochrome *c* (1:500 dilution) [31], rabbit-anti-*L. amazonensis* SODA and SODB (1:500), rabbit-anti-*L. major* ISCL (1:500) [33], and rabbit-anti-*Leishmania* HSP83 (1:5000) antisera [7]. The goat-anti-rabbit IgG conjugated with HRP (1:5000) was used as secondary antibody.

Measurement of oxygen consumption and ATP production

Oxygen consumption was determined using the MitoXpress Intracellular Oxygen Assay kit (Luxcel Biosciences, Cork, Ireland) as described previously [44]. Briefly, log phase parasites were washed and resuspended in DMEM or a mitochondrial respiration buffer (5.5 mM of sodium pyruvate, 5.5 mM of deoxy-D-glucose in Hank's Balanced Salt Solution or HBSS, pH 7.2) at 2 x 10^7 cells/ ml. For each sample, 100 µl of parasite suspension was added in triplicates in a 96 black-well microtiter plate. WT parasites pre-treated with 10 µM of antimycin A or 75 µM of CCCp were used as negative controls. 10 µl of MitoXpress (1 µM) was added to each well. A layer of mineral oil (100 µl/well) was added over the cells to prevent diffusion of atmospheric oxygen. MitoXpress signal was measured at 90s intervals for 60 min using excitation/emission wavelengths of 380 nm/650 nm in a BioTek synergy 4 fluorescence microplate reader. For each cell line, the relative OCR was calculated by subtracting the 0 min reading from the peak reading and then divided by the number of minutes this cell line needed to reach the peak.

To measure ATP production, parasites were washed and resuspended in a respiration buffer (21 mM of HEPES, 0.7 mM of Na_2HPO4, 137 mM of NaCl, pH 7.2) in the presence or absence of 5.5 mM of glucose or 5.5 mM of sodium pyruvate at 4 x 10^6 cells/ml. After incubation at 27 °C for 1 h or 4 h, 25 µl of suspension (corresponding to 1 x 10^5 cells) were transferred to a 96 black-well plate, mixed with equal volume of the CellTiter-Glo reagent (Promega) and incubated for 10 min in the dark. Bioluminescence was measured using a DTX 880 microplate reader as described [22]. For each assay, an ATP standard curve was prepared by diluting pure ATP stock in the respiration buffer. Parasites treated with 10 µM of antimycin A or 20 mM of sodium azide were included as controls.

Microscopy

To stain mitochondria, live parasites were resuspended in Dulbecco's Modified Eagle Medium (DMEM) at 1×10^6 cells/ml and labeled with 100 nM of Mitotracker CMXRos or TMRE. After incubation at 27 °C (30 min for Mitotracker and 15 min for TRME), parasites were washed once with PBS, fixed and processed for fluorescence microscopy as previously described [14]. MitoSox Red labeling (5 µM for 25 min at 27 °C) of live parasites was performed similarly without fixation using an Olympus BX51 Upright Fluorescence Microscope. DNA was stained with DAPI (2.5 µg/ml). Transmission electron microscopy of log and stationary phase promastigotes was performed as previously described [73].

Starvation and heat stress assays

To measure heat sensitivity, log phase promastigotes (2.5×10^6 cells/ml) were incubated in complete M199 media for 0-24 h at either 27 °C or 37 °C/5% CO_2. Effects of antimycin A (10 µM) and GSH (1 mM or 5 mM) on heat sensitivity were also monitored. For starvation response, log phase promastigotes were washed once in HBSS and resuspended in HBSS supplemented with glucose (5.5 mM), 2-deoxyglucose, (5.5 mM), aspartate (5.5 mM), sodium pyruvate (5.5 mM), or glycerol (0.1 mM) at 2.5×10^6 cells/ml and incubated for 0-24 h at 27 °C. In these stress assays, culture density over time was determined using a hemocytometer and percentage of dead cells was determined by flow cytometry following propidium iodide staining at 5 µg/ml [74].

Glucose and glycerol uptake assays

Uptake of glucose and glycerol were monitored as previously described with minor modifications [51, 75]. For glucose incorporation, log phase promastigotes were washed twice with PBS and resuspended at 5×10^7 cells/ml in PBS in the presence of 100 µM of D-[U-^{14}C] glucose (250 mCi/mmol, PerkinElmer Inc.). The reaction mixture (200 µl each in triplicates) was immediately loaded onto 100 µl of dibutyl phthalate in 1.5 ml Eppendorf tubes. Incubation was

performed at room temperature and terminated at the indicated times by pelleting cells through the oil layer through centrifugation (16000 g, 1 min). Tubes were then flash frozen in liquid nitrogen and the bottoms (containing cell pellets) were clipped off and submerged in scintillation fluid containing 1% SDS for 24 h, followed scintillation counting. To measure glycerol uptake, log phase promastigotes were washed twice in a transport buffer (33 mM of HEPES, 98 mM of NaCl, 4.6 mM of KCl, 0.55 mM of $CaCl_2$, 0.07 mM of $MgSO_4$, 5.8 mM of Na_2PO4, 0.3 mM of $NaHCO_3$, and 14 mM of glucose, pH 7.3) and resuspended at 1 x 10^8 cells/ml in the transport buffer. Uptake was measured at room temperature by mixing 100 µl of cells with 100 µl of transport buffer containing 8 µM of [^{14}C] glycerol (0.125 µCi each in triplicates, PerkinElmer Inc.). Incorporation of radioactivity was determined as described above.

Statistical analysis

Unless specified otherwise, assay values in all figures are averaged from three to five independent repeats and error bars represent standard deviations. Differences were assessed by the Student's t test (for two groups) or one-way ANOVA (for three or more groups) using the Sigmaplot 13.0 software (Systat Software Inc, San Jose, CA). *P* values indicating statistical significance were grouped (***: $p < 0.001$, **: $p < 0.01$, *: $p < 0.05$).

ACKNOWLEDGMENTS

We thank Dr. Norma Andrews (University of Maryland College Park) for providing us the rabbit anti-*L. amazonensis* SODA and SODB antisera, Dr. Wandy Beatty (Washington University in St. Louis) for transmission electron microscopy, and Dr. Catherine Wakeman for usage on the BioTek synergy 4 fluorescence microplate reader.

REFERENCES

1. Alvar J, Velez ID, Bern C, Herrero M, Desjeux P, Cano J, et al. Leishmaniasis worldwide and global estimates of its incidence. PloS one. 2012;7(5):e35671. Epub 2012/06/14. doi: 10.1371/journal.pone.0035671. PubMed PMID: 22693548; PubMed Central PMCID: PMC3365071.

2. Ghorbani M, Farhoudi R. Leishmaniasis in humans: drug or vaccine therapy? Drug Des Devel Ther. 2018;12:25-40. Epub 2018/01/11. doi: 10.2147/DDDT.S146521. PubMed PMID: 29317800; PubMed Central PMCID: PMCPMC5743117.

3. Croft SL, Sundar S, Fairlamb AH. Drug resistance in leishmaniasis. Clin Microbiol Rev. 2006;19(1):111-26. PubMed PMID: 16418526.

4. Goad LJ, Holz GG, Jr., Beach DH. Sterols of Leishmania species. Implications for biosynthesis. Mol Biochem Parasitol. 1984;10(2):161-70. Epub 1984/02/01. PubMed PMID: 6700638.

5. Urbina JA. Lipid biosynthesis pathways as chemotherapeutic targets in kinetoplastid parasites. Parasitology. 1997;114 Suppl:S91-9. PubMed PMID: 9309771.

6. Urbina JA, Vivas J, Lazardi K, Molina J, Payares G, Piras MM, et al. Antiproliferative effects of delta 24(25) sterol methyl transferase inhibitors on Trypanosoma (Schizotrypanum) cruzi: in vitro and in vivo studies. Chemotherapy. 1996;42(4):294-307. PubMed PMID: 8804798.

7. Xu W, Hsu FF, Baykal E, Huang J, Zhang K. Sterol Biosynthesis Is Required for Heat Resistance but Not Extracellular Survival in Leishmania. PLoS Pathog. 2014;10(10):e1004427. Epub 2014/10/24. doi: 10.1371/journal.ppat.1004427. PubMed PMID: 25340392.

8. de Souza W, Rodrigues JC. Sterol Biosynthesis Pathway as Target for Anti-trypanosomatid Drugs. Interdiscip Perspect Infect Dis. 2009;2009:642502. Epub 2009/08/15. doi: 10.1155/2009/642502. PubMed PMID: 19680554; PubMed Central PMCID: PMC2721973.

9. de Macedo-Silva ST, de Souza W, Rodrigues JC. Sterol Biosynthesis Pathway as an Alternative for the Anti-Protozoan Parasite Chemotherapy. Curr Med Chem. 2015;22(18):2186-98. Epub 2015/03/20. PubMed PMID: 25787966.

10. Jefcoate CR, Gaylor JL, Calabrese RL. Ligand interactions with cytochrome P-450. I. Binding of primary amines. Biochemistry. 1969;8(8):3455-63. Epub 1969/08/01. PubMed PMID: 5809236.

11. Warrilow AG, Parker JE, Kelly DE, Kelly SL. Azole affinity of sterol 14alpha-demethylase (CYP51) enzymes from Candida albicans and Homo sapiens. Antimicrob Agents Chemother. 2013;57(3):1352-60. Epub 2013/01/01. doi: 10.1128/AAC.02067-12. PubMed PMID: 23274672; PubMed Central PMCID: PMC3591892.

12. McCall LI, El Aroussi A, Choi JY, Vieira DF, De Muylder G, Johnston JB, et al. Targeting Ergosterol biosynthesis in Leishmania donovani: essentiality of sterol 14 alpha-demethylase. PLoS Negl Trop Dis. 2015;9(3):e0003588. Epub 2015/03/15. doi: 10.1371/journal.pntd.0003588. PubMed PMID: 25768284; PubMed Central PMCID: PMC4359151.

13. McConville MJ, Thomas-Oates JE, Ferguson MA, Homans SW. Structure of the lipophosphoglycan from Leishmania major. J Biol Chem. 1990;265(32):19611-23.

14. Mukherjee S, Xu W, Hsu FF, Patel J, Huang J, Zhang K. Sterol methyltransferase is required for optimal mitochondrial function and virulence in Leishmania major. Mol Microbiol.

2019;111(1):65-81. doi: 10.1111/mmi.14139. PubMed PMID: 30260041; PubMed Central PMCID: PMC6351164.

15. Dufourc EJ. Sterols and membrane dynamics. J Chem Biol. 2008;1(1-4):63-77. Epub 2009/07/02. doi: 10.1007/s12154-008-0010-6. PubMed PMID: 19568799; PubMed Central PMCID: PMC2698314.

16. Barenholz Y. Cholesterol and other membrane active sterols: from membrane evolution to "rafts". Prog Lipid Res. 2002;41(1):1-5. Epub 2001/11/06. PubMed PMID: 11694266.

17. Zinser E, Paltauf F, Daum G. Sterol composition of yeast organelle membranes and subcellular distribution of enzymes involved in sterol metabolism. J Bacteriol. 1993;175(10):2853-8. Epub 1993/05/01. PubMed PMID: 8491706; PubMed Central PMCID: PMC204601.

18. van Meer G, de Kroon AI. Lipid map of the mammalian cell. J Cell Sci. 2011;124(Pt 1):5-8. Epub 2010/12/22. doi: 10.1242/jcs.071233. PubMed PMID: 21172818.

19. Maxfield FR, Menon AK. Intracellular sterol transport and distribution. Curr Opin Cell Biol. 2006;18(4):379-85. Epub 2006/06/30. doi: 10.1016/j.ceb.2006.06.012. PubMed PMID: 16806879.

20. Rodrigues CO, Catisti R, Uyemura SA, Vercesi AE, Lira R, Rodriguez C, et al. The sterol composition of Trypanosoma cruzi changes after growth in different culture media and results in different sensitivity to digitonin-permeabilization. J Eukaryot Microbiol. 2001;48(5):588-94. Epub 2001/10/13. PubMed PMID: 11596924.

21. Kessler RL, Soares MJ, Probst CM, Krieger MA. Trypanosoma cruzi response to sterol biosynthesis inhibitors: morphophysiological alterations leading to cell death. PloS one.

2013;8(1):e55497. Epub 2013/02/06. doi: 10.1371/journal.pone.0055497. PubMed PMID: 23383204; PubMed Central PMCID: PMC3561218.

22. Perez-Moreno G, Sealey-Cardona M, Rodrigues-Poveda C, Gelb MH, Ruiz-Perez LM, Castillo-Acosta V, et al. Endogenous sterol biosynthesis is important for mitochondrial function and cell morphology in procyclic forms of Trypanosoma brucei. Int J Parasitol. 2012;42(11):975-89. Epub 2012/09/12. doi: 10.1016/j.ijpara.2012.07.012. PubMed PMID: 22964455.

23. Vannier-Santos MA, Urbina JA, Martiny A, Neves A, de Souza W. Alterations induced by the antifungal compounds ketoconazole and terbinafine in Leishmania. J Eukaryot Microbiol. 1995;42(4):337-46. Epub 1995/07/01. PubMed PMID: 7620457.

24. de Macedo-Silva ST, Urbina JA, de Souza W, Rodrigues JC. In vitro activity of the antifungal azoles itraconazole and posaconazole against Leishmania amazonensis. PloS one. 2013;8(12):e83247. Epub 2014/01/01. doi: 10.1371/journal.pone.0083247. PubMed PMID: 24376670; PubMed Central PMCID: PMC3871555.

25. Rodrigues JC, Attias M, Rodriguez C, Urbina JA, Souza W. Ultrastructural and biochemical alterations induced by 22,26-azasterol, a delta(24(25))-sterol methyltransferase inhibitor, on promastigote and amastigote forms of Leishmania amazonensis. Antimicrob Agents Chemother. 2002;46(2):487-99. PubMed PMID: 11796362.

26. Rodrigues JC, Bernardes CF, Visbal G, Urbina JA, Vercesi AE, de Souza W. Sterol methenyl transferase inhibitors alter the ultrastructure and function of the Leishmania amazonensis mitochondrion leading to potent growth inhibition. Protist. 2007;158(4):447-56. PubMed PMID: 17719843.

27. Orlandi PA, Jr., Turco SJ. Structure of the lipid moiety of the Leishmania donovani lipophosphoglycan. J Biol Chem. 1987;262(21):10384-91.

28. Stephens JL, Lee SH, Paul KS, Englund PT. Mitochondrial fatty acid synthesis in Trypanosoma brucei. J Biol Chem. 2007;282(7):4427-36. Epub 2006/12/15. doi: 10.1074/jbc.M609037200. PubMed PMID: 17166831.

29. Tomas AM, Castro H. Redox metabolism in mitochondria of trypanosomatids. Antioxid Redox Signal. 2013;19(7):696-707. Epub 2012/10/03. doi: 10.1089/ars.2012.4948. PubMed PMID: 23025438; PubMed Central PMCID: PMCPMC3739956.

30. Gros L, Lorente SO, Jimenez CJ, Yardley V, Rattray L, Wharton H, et al. Evaluation of azasterols as anti-parasitics. J Med Chemry. 2006;49(20):6094-103. Epub 2006/09/29. doi: 10.1021/jm060290f. PubMed PMID: 17004723.

31. Dolai S, Pal S, Yadav RK, Adak S. Endoplasmic reticulum stress-induced apoptosis in Leishmania through Ca2+-dependent and caspase-independent mechanism. J Biol Chem. 2011;286(15):13638-46. Epub 2011/02/19. doi: 10.1074/jbc.M110.201889. PubMed PMID: 21330370; PubMed Central PMCID: PMCPMC3075708.

32. Kathuria M, Bhattacharjee A, Sashidhara KV, Singh SP, Mitra K. Induction of mitochondrial dysfunction and oxidative stress in Leishmania donovani by orally active clerodane diterpene. Antimicrob Agents Chemother. 2014;58(10):5916-28. Epub 2014/07/30. doi: 10.1128/AAC.02459-14. PubMed PMID: 25070112; PubMed Central PMCID: PMC4187897.

33. Zhang O, Xu, W., Pillai, A., Zhang, K. Developmentally Regulated Sphingolipid Degradation in *Leishmania major*. PloS one. 2012;7(1):e31059.

34. Shapira M, Pinelli E. Heat-shock protein 83 of Leishmania mexicana amazonensis is an abundant cytoplasmic protein with a tandemly repeated genomic arrangement. Eur J Biochem. 1989;185(2):231-6. Epub 1989/11/06. PubMed PMID: 2684665.

35. Hide M, Ritleng AS, Brizard JP, Monte-Allegre A, Sereno D. Leishmania infantum: tuning digitonin fractionation for comparative proteomic of the mitochondrial protein content. Parasitol Res. 2008;103(4):989-92. Epub 2008/06/26. doi: 10.1007/s00436-008-1062-9. PubMed PMID: 18575891.

36. Drose S, Brandt U. Molecular mechanisms of superoxide production by the mitochondrial respiratory chain. AAdv Exp Med Biol. 2012;748:145-69. Epub 2012/06/26. doi: 10.1007/978-1-4614-3573-0_6. PubMed PMID: 22729857.

37. Kowaltowski AJ, de Souza-Pinto NC, Castilho RF, Vercesi AE. Mitochondria and reactive oxygen species. Free Radic Biol Med. 2009;47(4):333-43. Epub 2009/05/12. doi: 10.1016/j.freeradbiomed.2009.05.004. PubMed PMID: 19427899.

38. Liu Y, Fiskum G, Schubert D. Generation of reactive oxygen species by the mitochondrial electron transport chain. J Neurochem. 2002;80(5):780-7. Epub 2002/04/12. PubMed PMID: 11948241.

39. Moreira W, Leprohon P, Increased glycolytic ATP synthesis is associated with tafenoquine resistance in Leishmania majorOuellette M. Tolerance to drug-induced cell death favours the acquisition of multidrug resistance in Leishmania. Cell Death Dis. 2011;2:e201. Epub 2011/09/02. doi: 10.1038/cddis.2011.83. PubMed PMID: 21881603; PubMed Central PMCID: PMCPMC3186901.

40. Brand MD, Affourtit C, Esteves TC, Green K, Lambert AJ, Miwa S, et al. Mitochondrial superoxide: production, biological effects, and activation of uncoupling proteins. Free Radic Biol Med. 2004;37(6):755-67. Epub 2004/08/12. doi: 10.1016/j.freeradbiomed.2004.05.034. PubMed PMID: 15304252.

41. Fairlamb AH, Cerami A. Metabolism and functions of trypanothione in the Kinetoplastida. Annual review of microbiology. 1992;46:695-729. Epub 1992/01/01. doi: 10.1146/annurev.mi.46.100192.003403. PubMed PMID: 1444271.

42. Mittra B, Laranjeira-Silva MF, Miguel DC, Perrone Bezerra de Menezes J, Andrews NW. The iron-dependent mitochondrial superoxide dismutase SODA promotes Leishmania virulence. J Biol Chem. 2017;292(29):12324-38. Epub 2017/05/28. doi: 10.1074/jbc.M116.772624. PubMed PMID: 28550086; PubMed Central PMCID: PMC5519379.

43. Plewes KA, Barr SD, Gedamu L. Iron superoxide dismutases targeted to the glycosomes of Leishmania chagasi are important for survival. Infection and immunity. 2003;71(10):5910-20. Epub 2003/09/23. doi: 10.1128/iai.71.10.5910-5920.2003. PubMed PMID: 14500512; PubMed Central PMCID: PMCPMC201062.

44. Cardenas D, Carter PM, Nation CS, Pizarro JC, Guidry J, Aiyar A, et al. LACK, a RACK1 ortholog, facilitates cytochrome c oxidase subunit expression to promote Leishmania major fitness. Mol Microbiol. 2015;96(1):95-109. Epub 2015/01/15. doi: 10.1111/mmi.12924. PubMed PMID: 25582232; PubMed Central PMCID: PMC6055511.

45. Manzano JI, Carvalho L, Perez-Victoria JM, Castanys S, Gamarro F. Increased glycolytic ATP synthesis is associated with tafenoquine resistance in Leishmania major. Antimicrob Agents Chemother. 2011;55(3):1045-52. Epub 2011/01/05. doi: 10.1128/AAC.01545-10. PubMed PMID: 21199921; PubMed Central PMCID: PMCPMC3067095.

46. Guidarelli A, Brambilla L, Rota C, Tomasi A, Cattabeni F, Cantoni O. The respiratory-chain poison antimycin A promotes the formation of DNA single-strand breaks and reduces toxicity in U937 cells exposed to t-butylhydroperoxide. Biochem J. 1996;317 (Pt 2):371-5. Epub

1996/07/15. doi: 10.1042/bj3170371. PubMed PMID: 8713060; PubMed Central PMCID: PMCPMC1217497.

47. Leary SC, Hill BC, Lyons CN, Carlson CG, Michaud D, Kraft CS, et al. Chronic treatment with azide in situ leads to an irreversible loss of cytochrome c oxidase activity via holoenzyme dissociation. J Biol Chem. 2002;277(13):11321-8. Epub 2002/01/18. doi: 10.1074/jbc.M112303200. PubMed PMID: 11796734.

48. Pineda E, Thonnus M, Mazet M, Mourier A, Cahoreau E, Kulyk H, et al. Glycerol supports growth of the Trypanosoma brucei bloodstream forms in the absence of glucose: Analysis of metabolic adaptations on glycerol-rich conditions. PLoS Pathog. 2018;14(11):e1007412. Epub 2018/11/02. doi: 10.1371/journal.ppat.1007412. PubMed PMID: 30383867; PubMed Central PMCID: PMC6245841.

49. Kovarova J, Nagar R, Faria J, Ferguson MAJ, Barrett MP, Horn D. Gluconeogenesis using glycerol as a substrate in bloodstream-form Trypanosoma brucei. PLoS Pathog. 2018;14(12):e1007475. Epub 2018/12/28. doi: 10.1371/journal.ppat.1007475. PubMed PMID: 30589893; PubMed Central PMCID: PMCPMC6307712.

50. Feng X, Tran KD, Sanchez MA, Al Mezewghi H, Landfear SM. Glucose Transporters and Virulence in Leishmania mexicana. mSphere. 2018;3(4). Epub 2018/08/03. doi: 10.1128/mSphere.00349-18. PubMed PMID: 30068561; PubMed Central PMCID: PMC6070740.

51. Jeacock L, Baker N, Wiedemar N, Maser P, Horn D. Aquaglyceroporin-null trypanosomes display glycerol transport defects and respiratory-inhibitor sensitivity. PLoS Pathog. 2017;13(3):e1006307. Epub 2017/03/31. doi: 10.1371/journal.ppat.1006307. PubMed PMID: 28358927; PubMed Central PMCID: PMCPMC5388498.

52. Burchmore RJ, Rodriguez-Contreras D, McBride K, Merkel P, Barrett MP, Modi G, et al. Genetic characterization of glucose transporter function in Leishmania mexicana. Proc Natl Acad Sci U S A. 2003;100(7):3901-6. PubMed PMID: 12651954.

53. Mesmin B, Maxfield FR. Intracellular sterol dynamics. Biochim Biophys Acta. 2009;1791(7):636-45. Epub 2009/03/17. doi: 10.1016/j.bbalip.2009.03.002. PubMed PMID: 19286471; PubMed Central PMCID: PMCPMC2696574.

54. Figarella K, Marsiccobetre S, Arocha I, Colina W, Hasegawa M, Rodriguez M, et al. Ergosterone-coupled Triazol molecules trigger mitochondrial dysfunction, oxidative stress, and acidocalcisomal Ca(2+) release in Leishmania mexicana promastigotes. Microb Cell. 2015;3(1):14-28. Epub 2015/12/11. doi: 10.15698/mic2016.01.471. PubMed PMID: 28357313; PubMed Central PMCID: PMCPMC5354587.

55. van Meer G, Lisman Q. Sphingolipid transport: rafts and translocators. J Biol Chem. 2002;277(29):25855-8. PubMed PMID: 12011105.

56. Horvath SE, Daum G. Lipids of mitochondria. Prog Lipid Res. 2013;52(4):590-614. Epub 2013/09/07. doi: 10.1016/j.plipres.2013.07.002. PubMed PMID: 24007978.

57. Joshi AS, Thompson MN, Fei N, Huttemann M, Greenberg ML. Cardiolipin and mitochondrial phosphatidylethanolamine have overlapping functions in mitochondrial fusion in Saccharomyces cerevisiae. J Biol Chem. 2012;287(21):17589-97. Epub 2012/03/22. doi: 10.1074/jbc.M111.330167. PubMed PMID: 22433850; PubMed Central PMCID: PMC3366806.

58. Basu Ball W, Neff JK, Gohil VM. The role of nonbilayer phospholipids in mitochondrial structure and function. FEBS Lett. 2018;592(8):1273-90. Epub 2017/10/27. doi: 10.1002/1873-3468.12887. PubMed PMID: 29067684; PubMed Central PMCID: PMC5918238.

59. Hardie DG, Scott JW, Pan DA, Hudson ER. Management of cellular energy by the AMP-activated protein kinase system. FEBS Lett. 2003;546(1):113-20. Epub 2003/06/28. PubMed PMID: 12829246.

60. Carling D. The AMP-activated protein kinase cascade--a unifying system for energy control. TTrends Biochem Sci. 2004;29(1):18-24. Epub 2004/01/20. doi: 10.1016/j.tibs.2003.11.005. PubMed PMID: 14729328.

61. Chen L, Wang J, Zhang YY, Yan SF, Neumann D, Schlattner U, et al. AMP-activated protein kinase undergoes nucleotide-dependent conformational changes. Nat Struct Mol Biol. 2012;19(7):716-8. Epub 2012/06/05. doi: 10.1038/nsmb.2319. PubMed PMID: 22659875.

62. Roy A, Ganguly A, BoseDasgupta S, Das BB, Pal C, Jaisankar P, et al. Mitochondria-dependent reactive oxygen species-mediated programmed cell death induced by 3,3'-diindolylmethane through inhibition of F0F1-ATP synthase in unicellular protozoan parasite Leishmania donovani. Mol Pharmacol. 2008;74(5):1292-307. PubMed PMID: 18703668.

63. Basselin M, Denise H, Coombs GH, Barrett MP. Resistance to pentamidine in Leishmania mexicana involves exclusion of the drug from the mitochondrion. Antimicrob Agents Chemother. 2002;46(12):3731-8. Epub 2002/11/19. doi: 10.1128/aac.46.12.3731-3738.2002. PubMed PMID: 12435669; PubMed Central PMCID: PMCPMC132791.

64. Mukherjee A, Padmanabhan PK, Sahani MH, Barrett MP, Madhubala R. Roles for mitochondria in pentamidine susceptibility and resistance in Leishmania donovani. Mol Biochem Parasitol. 2006;145(1):1-10. Epub 2005/10/13. doi: 10.1016/j.molbiopara.2005.08.016. PubMed PMID: 16219371.

65. Pountain AW, Weidt SK, Regnault C, Bates PA, Donachie AM, Dickens NJ, et al. Genomic instability at the locus of sterol C24-methyltransferase promotes amphotericin B

resistance in Leishmania parasites. PLoS Negl Trop Dis. 2019;13(2):e0007052. Epub 2019/02/05. doi: 10.1371/journal.pntd.0007052. PubMed PMID: 30716073; PubMed Central PMCID: PMCPMC6375703.

66. Mwenechanya R, Kovarova J, Dickens NJ, Mudaliar M, Herzyk P, Vincent IM, et al. Sterol 14alpha-demethylase mutation leads to amphotericin B resistance in Leishmania mexicana. PLoS Negl Trop Dis. 2017;11(6):e0005649. Epub 2017/06/18. doi: 10.1371/journal.pntd.0005649. PubMed PMID: 28622334; PubMed Central PMCID: PMCPMC5498063.

67. Kapler GM, Coburn CM, Beverley SM. Stable transfection of the human parasite *Leishmania major* delineates a 30-kilobase region sufficient for extrachromosomal replication and expression. Mol Cell Biol. 1990;10(3):1084-94. PubMed PMID: 2304458.

68. Bates PA, Robertson CD, Tetley L, Coombs GH. Axenic cultivation and characterization of Leishmania mexicana amastigote-like forms. Parasitology. 1992;105 (Pt 2):193-202. Epub 1992/10/01. PubMed PMID: 1454417.

69. Zhang K, Showalter M, Revollo J, Hsu FF, Turk J, Beverley SM. Sphingolipids are essential for differentiation but not growth in *Leishmania*. EMBO J. 2003;22(22):6016-26. PMCID: 275442. PubMed PMID: 14609948.

70. Vergnes B, Gourbal B, Girard I, Sundar S, Drummelsmith J, Ouellette M. A proteomics screen implicates HSP83 and a small kinetoplastid calpain-related protein in drug resistance in Leishmania donovani clinical field isolates by modulating drug-induced programmed cell death. Mol Cell Proteomics. 2007;6(1):88-101. Epub 2006/10/20. doi: 10.1074/mcp.M600319-MCP200. PubMed PMID: 17050524.

71. Mittra B, Laranjeira-Silva MF, Perrone Bezerra de Menezes J, Jensen J, Michailowsky V, Andrews NW. A Trypanosomatid Iron Transporter that Regulates Mitochondrial Function Is Required for Leishmania amazonensis Virulence. PLoS Pathog. 2016;12(1):e1005340. Epub 2016/01/08. doi: 10.1371/journal.ppat.1005340. PubMed PMID: 26741360; PubMed Central PMCID: PMC4704735.

72. Kaser S, Oeljeklaus S, Tyc J, Vaughan S, Warscheid B, Schneider A. Outer membrane protein functions as integrator of protein import and DNA inheritance in mitochondria. Proc Natl Acad Sci U S A. 2016;113(31):E4467-75. Epub 2016/07/21. doi: 10.1073/pnas.1605497113. PubMed PMID: 27436903; PubMed Central PMCID: PMCPMC4978248.

73. Zhang K, Hsu FF, Scott DA, Docampo R, Turk J, Beverley SM. *Leishmania* salvage and remodelling of host sphingolipids in amastigote survival and acidocalcisome biogenesis. Mol Microbiol. 2005;55(5):1566-78. PubMed PMID: 15720561.

74. Xu W, Xin L, Soong L, Zhang K. Sphingolipid degradation by Leishmania major is required for its resistance to acidic pH in the mammalian host. Infect Immun. 2011;79(8):3377-87. Epub 2011/05/18. doi: 10.1128/IAI.00037-11. PubMed PMID: 21576322; PubMed Central PMCID: PMC3147570.

75. Rodriguez-Contreras D, Landfear SM. Metabolic changes in glucose transporter-deficient Leishmania mexicana and parasite virulence. J Biol Chem. 2006;281(29):20068-76. PubMed PMID: 16707495.

FIGURE CAPTIONS

Fig 1. *C14dm*⁻ promastigotes show high mitochondrial membrane potential (ΔΨm). (**A**) Log phase promastigotes were labeled with 100 nM of Mitotracker CMXRos followed by DAPI staining. WT parasites pretreated with CCCp were included as controls. DIC: differential interference contrast. (**B**) Representative transmission electron micrographs showing mitochondria in log phase promastigotes. Black arrows indicate areas containing kinetoplast (top panel) and tubular mitochondria (bottom panel). (**C**) To measure ΔΨm, log phase and stationary phase (day 1-day 4) promastigotes were labelled with 100 nM of TMRE for 15 minutes in PBS and mean fluorescence intensity (MFI) were determined by flow cytometry. Controls include WT and *c14dm*⁻ parasites pretreated with CCCp and WT cells pretreated with 0.2 µM of ITZ. Bar values represent averages from three experiments and error bars represent standard deviations. **: $p<0.01$, *: $p<0.05$. (**D**) Live parasites imaging after TMRE labeling.

Fig 2. Inactivation of C14DM leads to ROS accumulation in the mitochondria. (**A**, **B** and **F**) Promastigotes were incubated in complete M199, serum-free M199, PBS contain 5.5 mM of glucose, or PBS only and labeled with 100 nM of TMRE (**A**, for 15 min), 5 µM of MitoSox Red (**B**, for 25 min) or 5 µM of DHE (**F**, for 30 min). MFIs were determined by flow cytometry. Effects of CCCp (75 µM, 15 min) were also monitored in **A** and **B**. (**C**) Log or stationary phase (day 1-day 4) promastigotes were labeled with 5 µM of MitoSox Red for 25 min in PBS and MFIs were determined by flow cytometry and normalized to values from log phase WT. WT cells grown in the presence of ITZ (for 48 hr) were also analyzed. (**D** and **E**) Live cell imaging of *L. major* promastigotes (**D**) or *Leishmania mexicana* axenic amastigotes (grown in the absence or presence of 0.1 µM of ITZ for 48 hr, **E**) after labelling with MitoSox Red in PBS. White arrows indicate kDNA binding of MitoSox. (**E**) Live after labeling with MitoSox Red. In **A-C** and **F**,

833 averaged values from five experiments are shown and error bars represent standard deviations.
834 ***: $p<0.001$, **: $p<0.01$, *: $p<0.05$.

835 **Fig 3. Increased superoxide dismutase (SOD) activity in *c14dm⁻* parasites.** (**A**) Whole cell
836 lysates from log phase and stationary phase (day 1 to day 3) promastigotes were collected as
837 described in Materials and Methods. SOD activity was measured using a SOD assay kit
838 (BioAssay Systems) and results were normalized based on the amount of protein in each sample.
839 Error bars represent standard deviations from two independent experiments (*: $p<0.05$). (**B**)
840 Mitochondria enriched membrane fractions (Mem.) and cytosolic fractions (Sup.) were isolated
841 from log phase promastigotes as described. Western blots were performed using antibodies
842 against *L. amazonensis* SODA (mitochondrial) and SODB (both SODB1 and SODB2,
843 glycosomal).

844 **Fig 4. *C14dm⁻* parasites show compromised cellular respiration.** (**A**) Log phase
845 promastigotes were incubated in HBSS buffer for 1 hour and oxygen consumption rates (OCR)
846 were determined as described in Materials and Methods. WT parasites treated with antimycin A
847 (AA) were included as controls. (**B**) Cellular ATP contents in log phase promastigotes were
848 measured after 1 hour incubation in HBSS in the absence or presence of glucose (Glu, 5.5 mM)
849 or sodium azide (NaN3, 20 mM). (**C**) Cellular ATP contents in log phase promastigotes were
850 measured after 1 hour or 4 hour incubation in HBSS in the absence or presence of sodium
851 pyruvate (Pyr, 5.5 mM) or AA (10 μM). All experiments were repeated three times and error
852 bars represent standard deviations. **: $p<0.01$, *: $p<0.05$.

853 **Fig 5. *C14dm⁻* parasites are hypersensitive to starvation.** Log phase promastigotes were
854 inoculated in HBSS in the absence or presence of 2-deoxyglucose (2DG, 5.5 mM), Pyr (5.5 mM),
855 aspartate (Asp, 5.5 mM), Glu (5.5 mM), or glycerol (0.1 mM). In **A**, percentages of cell death

were determined after 24 hours for WT, *c14dm⁻*, *c14dm⁻/+C14DM*, *smt⁻*, and *smt⁻/+SMT* parasites. In **B**, percentages of cell death for *c14dm⁻* mutants were determined at the indicated time points. Error bars represent standard deviations from three independent experiments (***: $p<0.001$, **: $p<0.01$).

Fig 6. *C14dm⁻* parasites show increased uptake of glucose and glycerol. Incorporation of radiolabeled glucose (**A**) or glycerol (**B** and **C**) were determined as described under Materials and Methods. Transport assays were performed at room temperature (**A** and **B** unless specified) or 4 °C (**C**). Error bars represent standard deviations from three independent experiments (***: $p<0.001$, **: $p<0.01$, *: $p<0.05$).

Fig 7. ROS accumulation contributes to heat sensitivity in *c14dm⁻* mutants. (**A**-**E**) Log phase promastigotes were incubated in PBS at 27 °C or 37 °C for 3 hours. In **A**, percentages of cell death were determined by flow cytometry after PI staining. In **B**, ΔΨm was determined after TMRE labeling. Unlabeled WT parasites were included as negative controls (Neg). In **C**-**D**, parasites were lysed and cytosolic fractions (Sup.) were separated from mitochondrial fractions (Mem.) as described in Materials and Methods. Distribution of cytochrome *c* and HSP83 (a cytosolic protein marker) were determined by Western blots (**C**) and quantified (**D**). In **E**, parasites were labelled with the cytosolic ROS indicator DHE. Fluorescence intensities were measured by flow cytometry and relative cytosolic ROS levels were determined. (**F**) Log phase promastigotes were incubated at 37 °C in the absence or presence of reduced GSH. After 8 hours, mitochondrial ROS levels were measured as described. (**G**) *C14dm⁻* parasites were incubated at 37 °C in the absence or presence of reduced GSH and percentages of cell death were determined at 0 and 8 hours. (**H**) WT parasites were incubated at 27 °C or 37 °C in the absence or presence of AA (10 μM) and percentages of dead cells were determined by flow cytometry at the

indicated time points. †: Very few WT+AA cells were detectable after 36 hours at 37 °C. Error bars represent standard deviations from three independent experiments (***: $p<0.001$, **: $p<0.01$, *: $p<0.05$).

SUPPLEMENTAL FIGURE CAPTIONS

Fig S1. *C14dm⁻* promastigotes show increased mitochondrial surface area but maintain mitochondrial membrane integrity at ambient temperature. (**A**) After Mitotracker staining (Fig 1A), the average mitochondrial surface areas in log phase promastigotes of WT, *c14dm⁻*, and *c14dm⁻/+C14DM* were determined using Image J (~200 cells were analyzed for each parasite line, au: arbitrary unit). (**B**) Log phase promastigotes were lysed with 0.035% of digitonin at 37 °C or room temperature (RT) and mitochondria enriched membrane fractions (Mem.) were separated from cytosolic fractions (Sup.) as described in Materials and Methods. Western blots were performed using antibodies against cytochrome *c*, ISCL (a mitochondrial membrane protein), and HSP83 (a cytosolic protein).

Fig S2. *C14dm⁻* mutants show increased ΔMΨ after staining with rhodamine. Log phase and stationary phase promastigotes were resuspended in PBS and labeled with 5 μg/ml of rhodamine 123 for 15 min at room temperature. MFIs were determined by flow cytometry. Error bars represent standard deviations from three independent experiments (**: $p<0.01$, *: $p<0.05$).

Fig S3. *C14dm⁻* mutants accumulate ROS in the mitochondria. Log phase promastigotes were labeled with 5 μM of MitoSox Red for 25 min (**A**) or 5 μM of DHE for 30 min (**B**) and MFIs were determined by flow cytometry. Effects of antimycin A (5 μM) and H_2O_2 (100 μM) on WT parasites were also monitored. Error bars represent standard deviations from three experiments.

Fig S4. 100 μM of glucose or glycerol is sufficient to rescue *c14dm⁻* mutants in PBS. Log phase promastigotes were incubated in PBS in the absence or presence of glucose (100 μM) or glycerol (100 μM) and percentages of dead cells were determined by flow cytometry at the indicated time points. Error bars represent standard deviations from three experiments.

Fig S5. ITZ-treated WT parasites are hypersensitive to glucose depletion. *L. major* WT promastigotes were cultivated in solvent alone (0.1% w/v of DMSO) or 0.2 μM of ITZ for 48 hours. Cells were then incubated in HBSS and percentages of dead cells were determined by flow cytometry at the indicated time points. Error bars represent standard deviations from three experiments (**: $p < 0.01$, ***: $p < 0.001$).

Fig S6. *C14dm⁻* mutants rescued by glucose or glycerol show less mitochondrial defects. Log phase promastigotes were incubated in PBS in the absence or presence of glucose (100 μM) or glycerol (100 μM) for 24 hours. ΔΦm (**A**) and mitochondrial ROS level (**B**) were determined by flow cytometry. Control cells represent cells analyzed at the beginning of incubation. †: no viable *c14dm⁻* mutants were available after 24 hours. Error bars represent standard deviations from three experiments (**: $p < 0.01$, ***: $p < 0.001$).

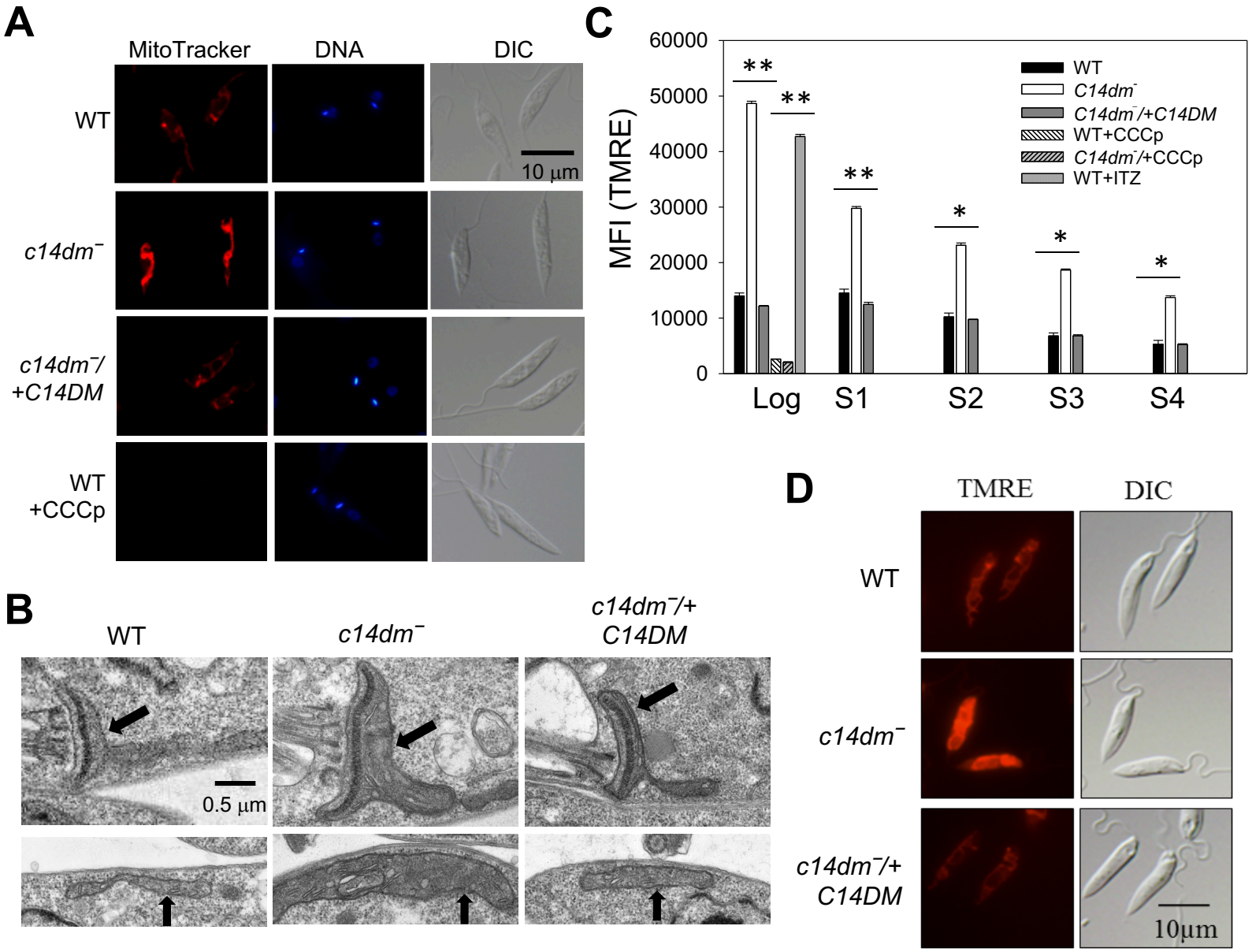

Figure 1. *C14dm⁻* promastigotes show high mitochondrial membrane potential (ΔΨm). (**A**) Log phase promastigotes were labeled with 100 nM of Mitotracker CMXRos followed by DAPI staining. WT parasites pretreated with CCCp were included as controls. DIC: differential interference contrast. (**B**) Representative transmission electron micrographs showing mitochondria in log phase promastigotes. Black arrows indicate areas containing kinetoplast (top panel) and tubular mitochondria (bottom panel). (**C**) To measure ΔΨm, log phase and stationary phase (day 1-day 4) promastigotes were labelled with 100 nM of TMRE for 15 minutes in PBS and mean fluorescence intensity (MFI) were determined by flow cytometry. Controls include WT and *c14dm⁻* parasites pretreated with CCCp and WT cells pretreated with 0.2 µM of ITZ. Bar values represent averages from three experiments and error bars represent standard deviations. **: $p<0.01$, *: $p<0.05$. (**D**) Live parasites imaging after TMRE labeling.

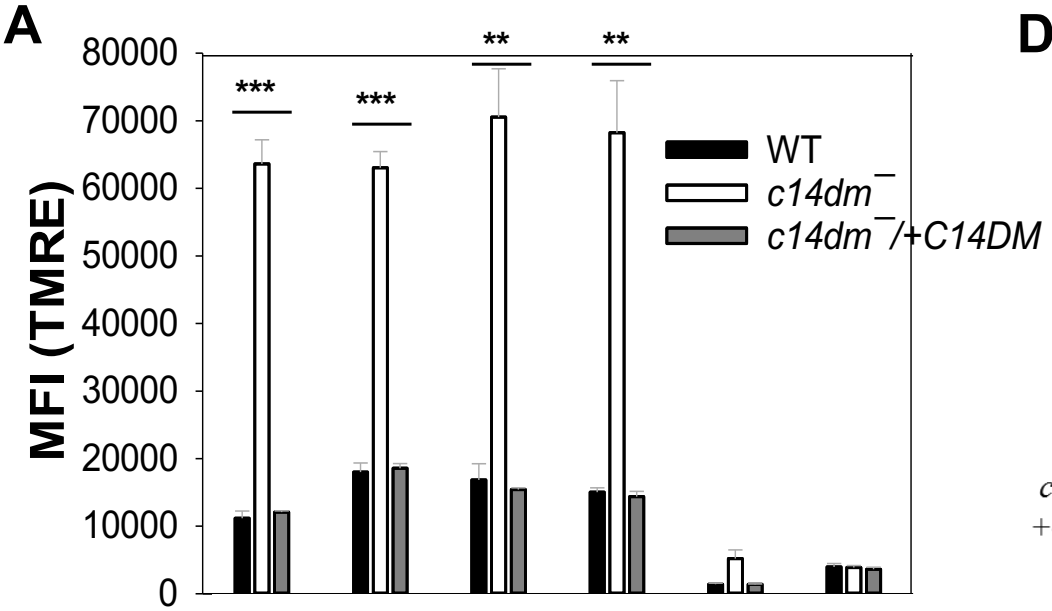
A
MFI (TMRE)
80000
70000
60000
50000
40000
30000
20000
10000
0
***
***
**
**
WT
c14dm⁻
c14dm⁻/+C14DM

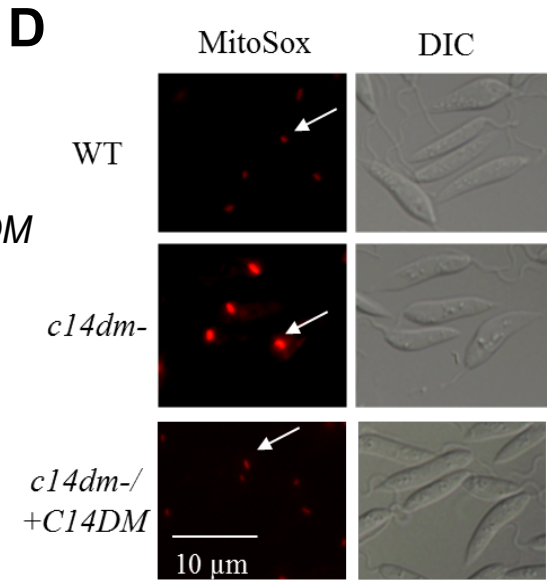
D
MitoSox
DIC
WT
c14dm-
c14dm-/
+C14DM
10 µm

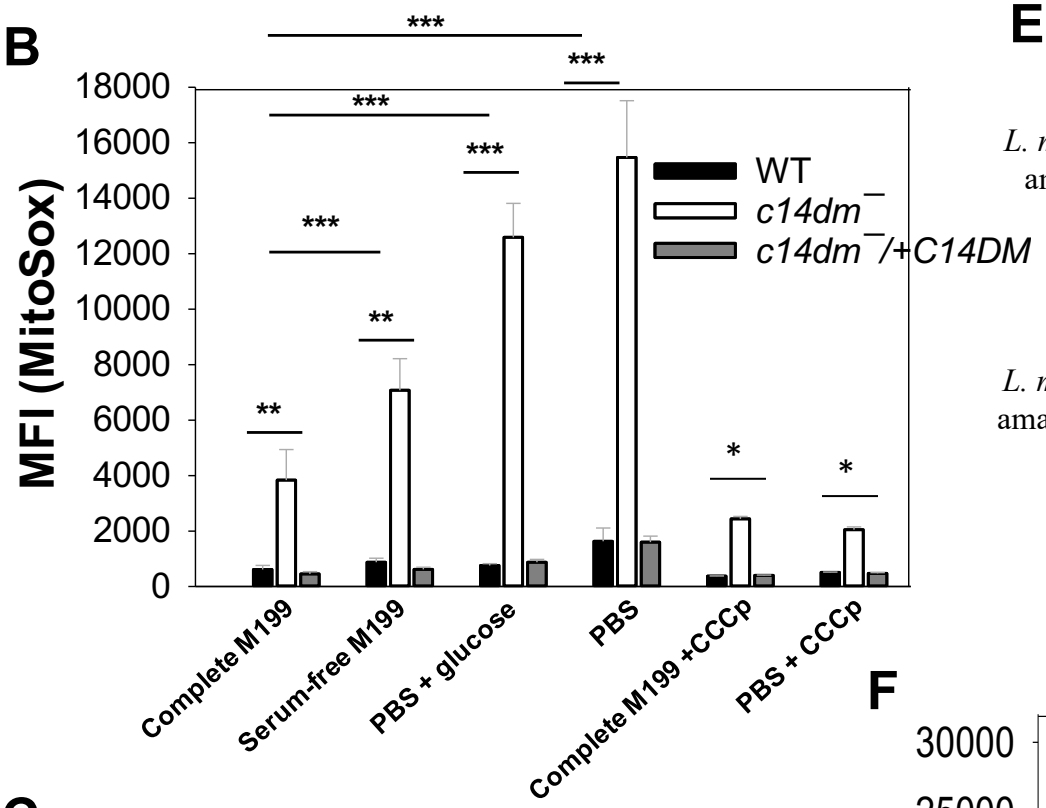
B
MFI (MitoSox)
18000
16000
14000
12000
10000
8000
6000
4000
2000
0
***
***
***
***
***
**
**
*
*
WT
c14dm⁻
c14dm⁻/+C14DM
Complete M199
Serum-free M199
PBS + glucose
PBS
Complete M199 +CCCp
PBS + CCCp

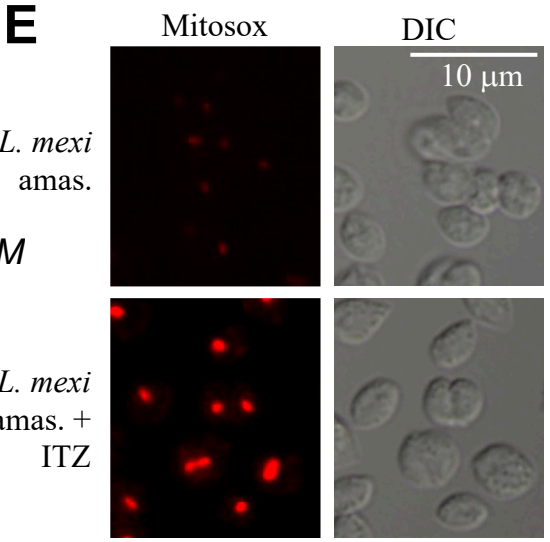
E
Mitosox
DIC
10 µm
L. mexi
amas.
L. mexi
amas. +
ITZ

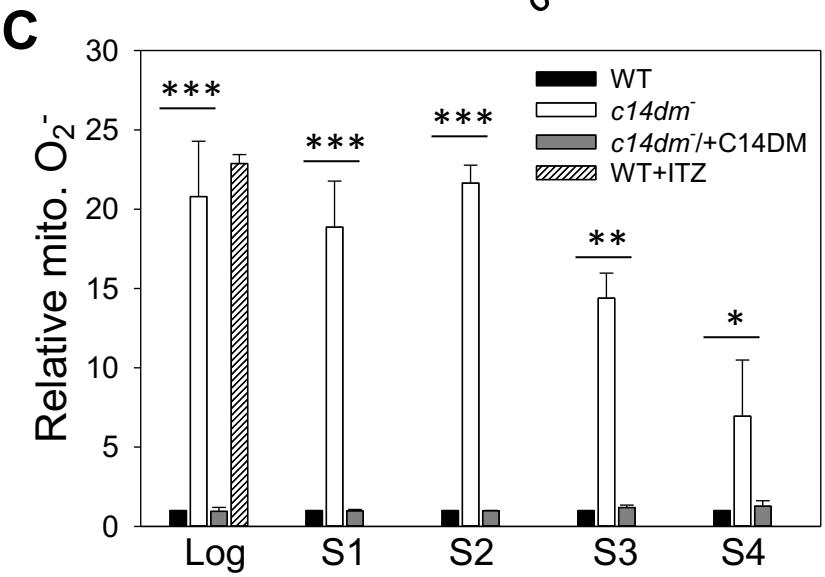
C
Relative mito. O2-
30
25
20
15
10
5
0
***
***
***
**
*
WT
c14dm-
c14dm-/+C14DM
WT+ITZ
Log
S1
S2
S3
S4

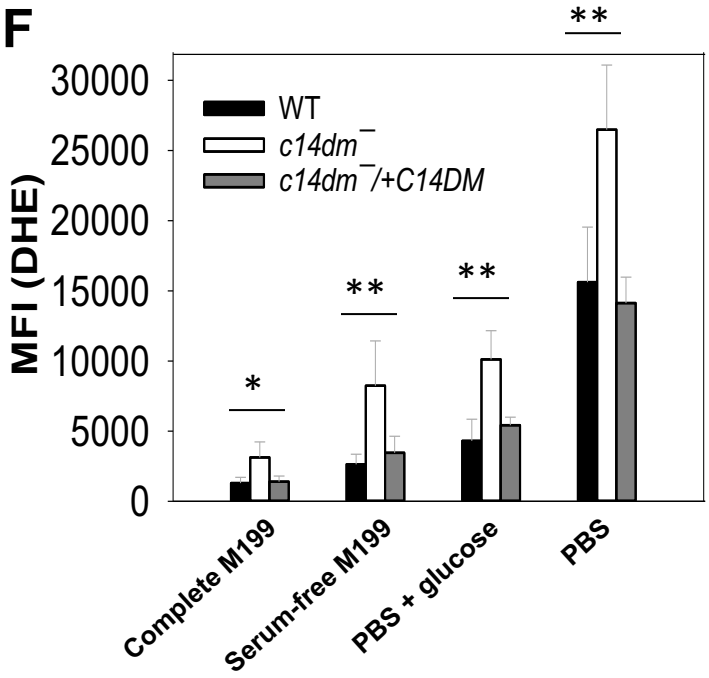
F
MFI (DHE)
30000
25000
20000
15000
10000
5000
0
*
**
**
**
WT
c14dm⁻
c14dm⁻/+C14DM
Complete M199
Serum-free M199
PBS + glucose
PBS

Figure 2. Inactivation of C14DM leads to ROS accumulation in the mitochondria. (**A**, **B** and **F**) Promastigotes were incubated in complete M199, serum-free M199, PBS contain 5.5 mM of glucose, or PBS only and labeled with 100 nM of TMRE (**A**, 15 min), 5 μM of MitoSox Red (**B**, 25 min) or 5 μM of DHE (**F**, 30 min). MFIs were determined by flow cytometry. Effects of CCCp (75 μM, 15 min) were also monitored in **A** and **B**. (**C**) Log or stationary phase (day 1-day 4) promastigotes were labeled with 5 μM of MitoSox Red for 25 min in PBS and MFIs were determined by flow cytometry and normalized to values from log phase WT. WT cells grown in the presence of ITZ (for 48 hr) were also analyzed. (**D** and **E**) Live cell imaging of *L. major* promastigotes (**D**) or *Leishmania mexicana* axenic amastigotes (grown in the absence or presence of 0.1 μM of ITZ for 48 hr, **E**) after labelling with MitoSox Red in PBS. White arrows indicate kDNA binding of MitoSox. (**E**) Live after labeling with MitoSox Red. In **A-C** and **F**, averaged values from five experiments are shown and error bars represent standard deviations. ***: $p<0.001$, **: $p<0.01$, *: $p<0.05$.

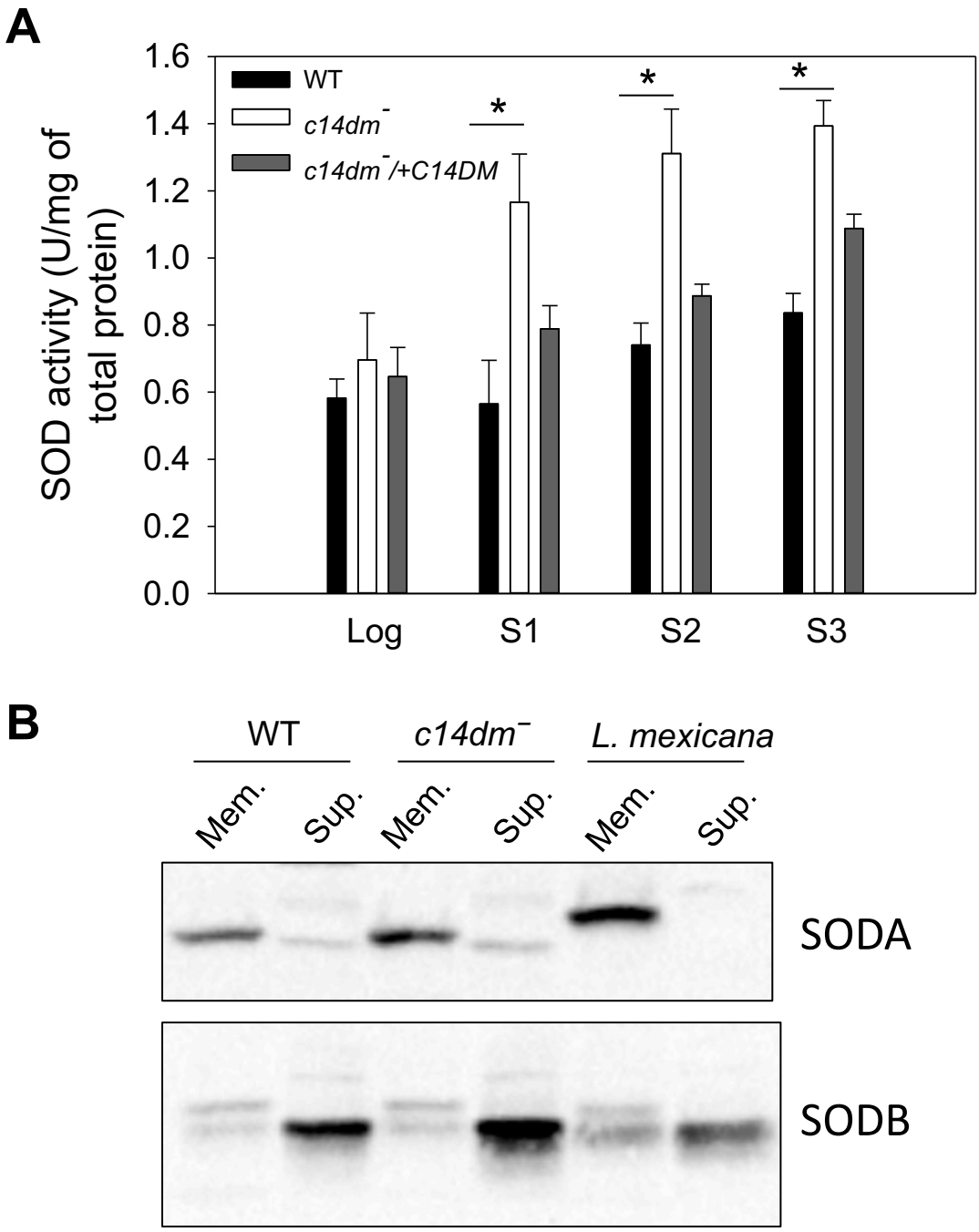

Figure 3. Increased superoxide dismutase (SOD) activity in *c14dm⁻* parasites. (**A**) Whole cell lysates from log phase and stationary phase (day 1 to day 3) promastigotes were collected as described in Materials and Methods. SOD activity was measured using a SOD assay kit (BioAssay Systems) and results were normalized based on the amount of protein in each sample. Error bars represent standard deviations from two independent experiments (*: $p<0.05$). (**B**) Mitochondria enriched membrane fractions (Mem.) and cytosolic fractions (Sup.) were isolated from log phase promastigotes as described. Western blots were performed using antibodies against *L. amazonesis* SODA (mitochondrial) and SODB (both SODB1 and SODB2, glycosomal).

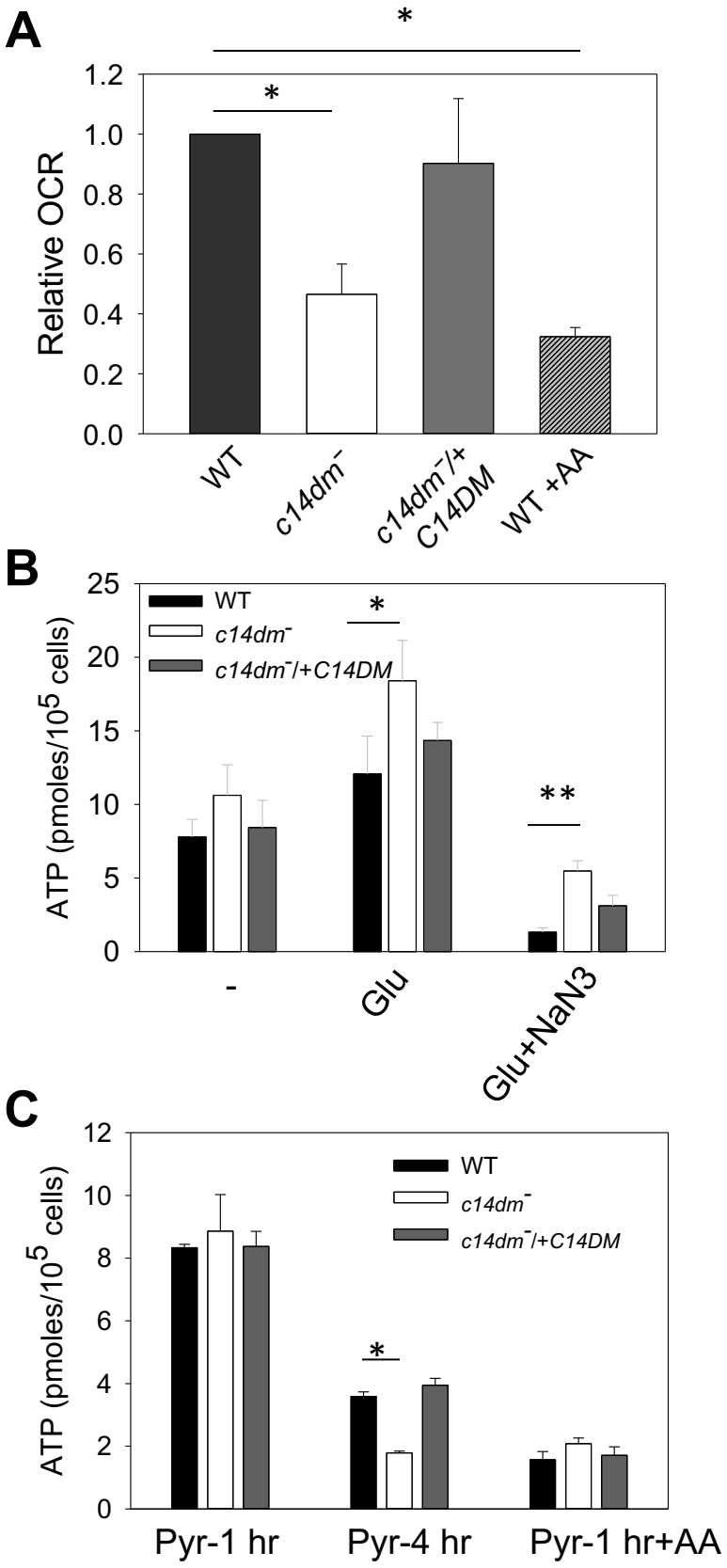

Figure 4. *C14dm⁻* parasites show compromised cellular respiration. (**A**) Log phase promastigotes were incubated in HBSS buffer for 1 hour and oxygen consumption rates (OCR) were determined as described in Materials and Methods. WT parasites treated with antimycin A (AA) were included as controls. (**B**) Cellular ATP contents in log phase promastigotes were measured after 1 hour incubation in HBSS in the absence or presence of glucose (Glu, 5.5 mM) or sodium azide (NaN3, 20 mM). (**C**) Cellular ATP contents in log phase promastigotes were measured after 1 hour or 4 hour incubation in HBSS in the absence or presence of sodium pyruvate (Pyr, 5.5 mM) or AA (10 μM). All experiments were repeated three times and error bars represent standard deviations. **: $p<0.01$, *: $p<0.05$.

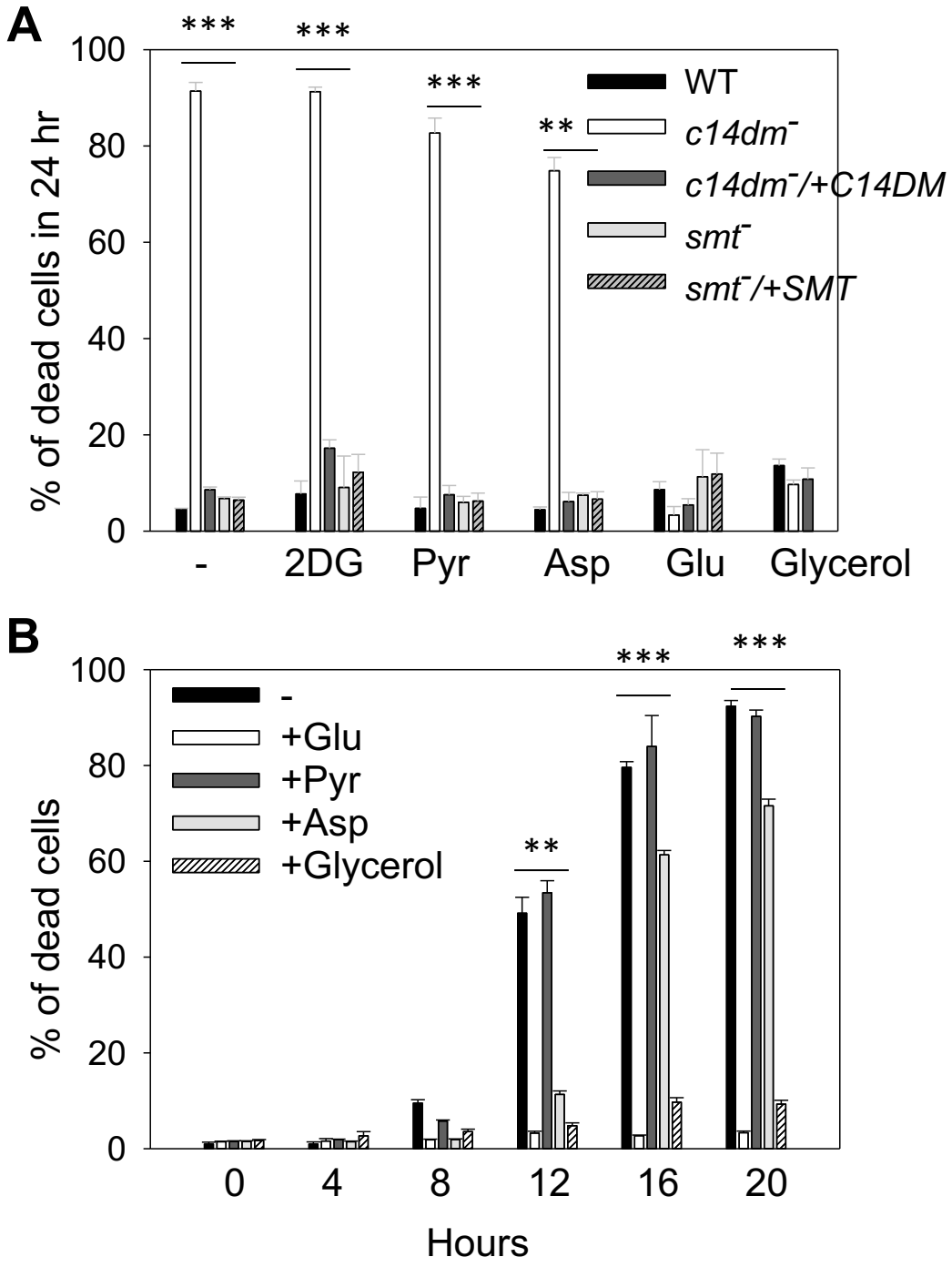

Figure 5. *C14dm⁻* parasites are hypersensitive to starvation. Log phase promastigotes were inoculated in HBSS in the absence or presence of 2-deoxyglucose (2DG, 5.5 mM), Pyr (5.5 mM), aspartate (Asp, 5.5 mM), Glu (5.5 mM), or glycerol (0.1 mM). In **A**, percentages of cell death were determined after 24 hours for WT, *c14dm⁻, c14dm⁻/+C14DM, smt⁻*, and *smt⁻/+SMT* parasites. In **B**, percentages of cell death for *c14dm⁻* mutants were determined at the indicated time points. Error bars represent standard deviations from three independent experiments (***: $p<0.001$, **: $p<0.01$).

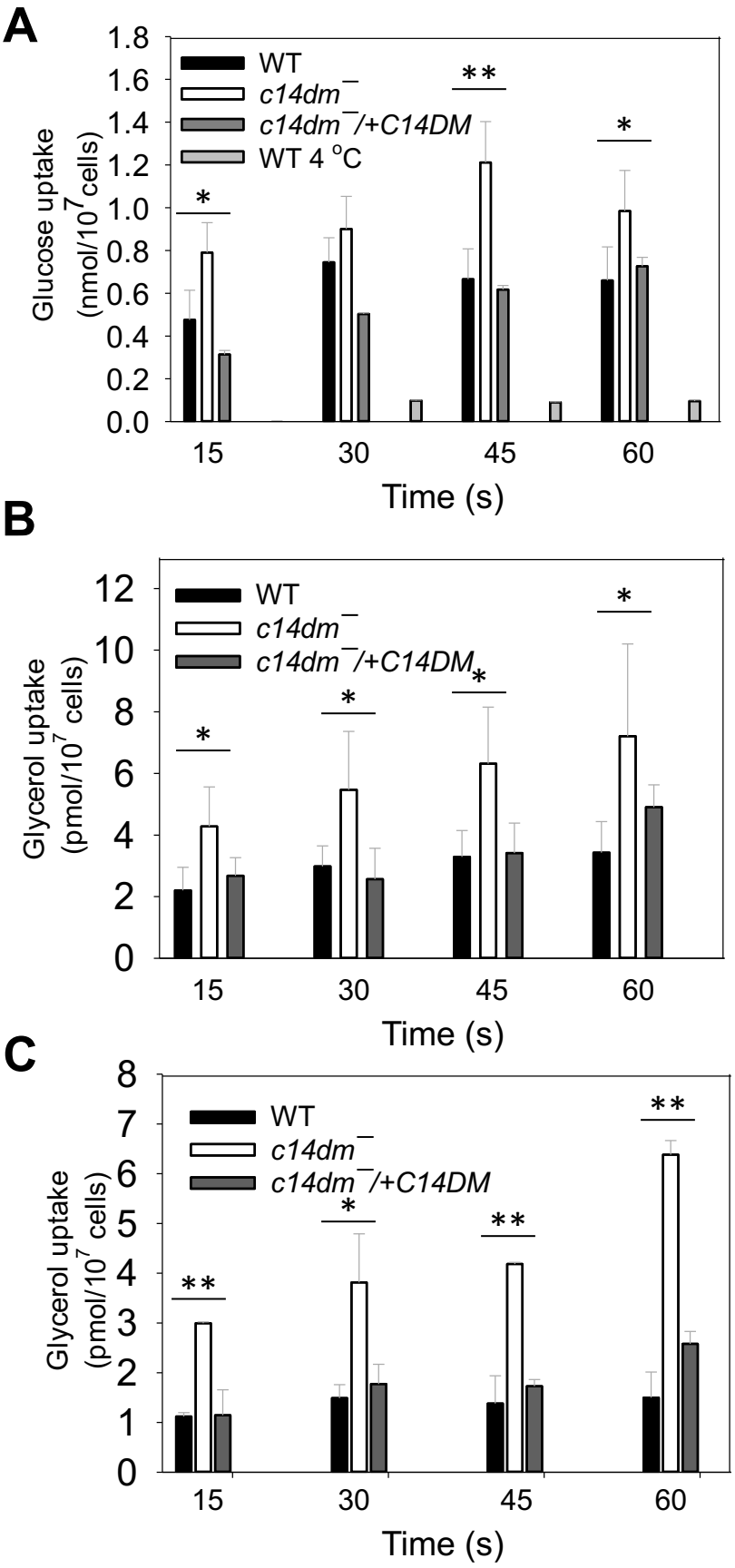

Figure 6. *C14dm⁻* parasites show increased uptake of glucose and glycerol. Incorporation of radiolabeled glucose (**A**) or glycerol (**B** and **C**) were determined as described under Materials and Methods. Transport assays were performed at room temperature (**A** and **B** unless specified) or 4 °C (**C**). Error bars represent standard deviations from three independent experiments (***: $p<0.001$, **: $p<0.01$).

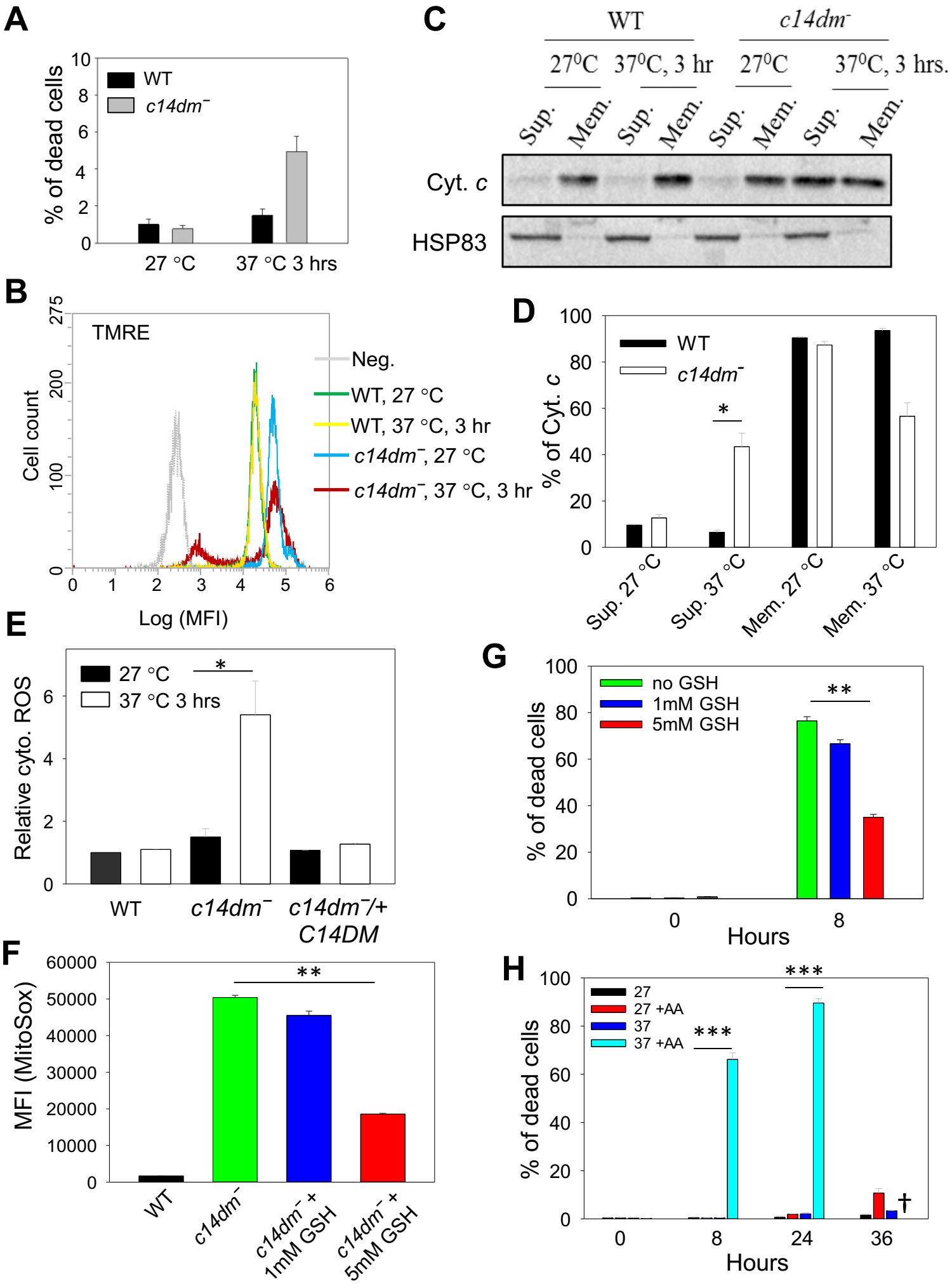
A
% of dead cells
WT
c14dm⁻
27 °C
37 °C 3 hrs
B
TMRE
Cell count
Log (MFI)
Neg.
WT, 27 °C
WT, 37 °C, 3 hr
c14dm⁻, 27 °C
c14dm⁻, 37 °C, 3 hr
C
WT
c14dm⁻
27⁰C
37⁰C, 3 hr
27⁰C
37⁰C, 3 hrs.
Sup.
Mem.
Cyt. c
HSP83
D
% of Cyt. c
WT
c14dm⁻
Sup. 27 °C
Sup. 37 °C
Mem. 27 °C
Mem. 37 °C
E
Relative cyto. ROS
27 °C
37 °C 3 hrs
WT
c14dm⁻
c14dm⁻/+ C14DM
F
MFI (MitoSox)
WT
c14dm⁻
c14dm⁻ + 1mM GSH
c14dm⁻ + 5mM GSH
G
% of dead cells
no GSH
1mM GSH
5mM GSH
Hours
H
% of dead cells
27
27 +AA
37
37 +AA
Hours

Figure 7. ROS accumulation contributes to heat sensitivity in *c14dm⁻* mutants. (**A**-**E**) Log phase promastigotes were incubated in PBS at 27 °C or 37 °C for 3 hours. In **A**, percentages of cell death were determined by flow cytometry after PI staining. In **B**, ΔΨm was determined after TMRE labeling. Unlabeled WT parasites were included as negative controls (Neg). In **C**-**D**, parasites were lysed and cytosolic fractions (Sup.) were separated from mitochondrial fractions (Mem.) as described in Materials and Methods. Distribution of cytochrome *c* and HSP83 (a cytosolic protein marker) were determined by Western blots (**C**) and quantified (**D**). In **E**, parasites were labelled with the cytosolic ROS indicator DHE. Fluorescence intensities were measured by flow cytometry and relative cytosolic ROS levels were determined. (**F**) Log phase promastigotes were incubated at 37 °C in the absence or presence of reduced GSH. After 8 hours, mitochondrial ROS levels were measured as described. (**G**) *C14dm⁻* parasites were incubated at 37 °C in the absence or presence of reduced GSH and percentages of cell death were determined at 0 and 8 hours. (**H**) WT parasites were incubated at 27 °C or 37 °C in the absence or presence of AA (10 μM) and percentages of dead cells were determined by flow cytometry at the indicated time points. †: Very few WT+AA cells were detectable after 36 hours at 37 °C. Error bars represent standard deviations from three independent experiments (***: $p<0.001$, **: $p<0.01$, *: $p<0.05$).